Department of Precision and Microsystems Engineering

Diamagnetically levitated resonant mass sensor

Nimit Kothari

Report no : 2019.022
Coach : Prof. Dr. P. G. Steeneken
Professor : Prof. Dr. P. G. Steeneken
Specialisation : Dynamics of Micro and Nanosystems
Type of report : Master Thesis
Date : 19 July, 2019

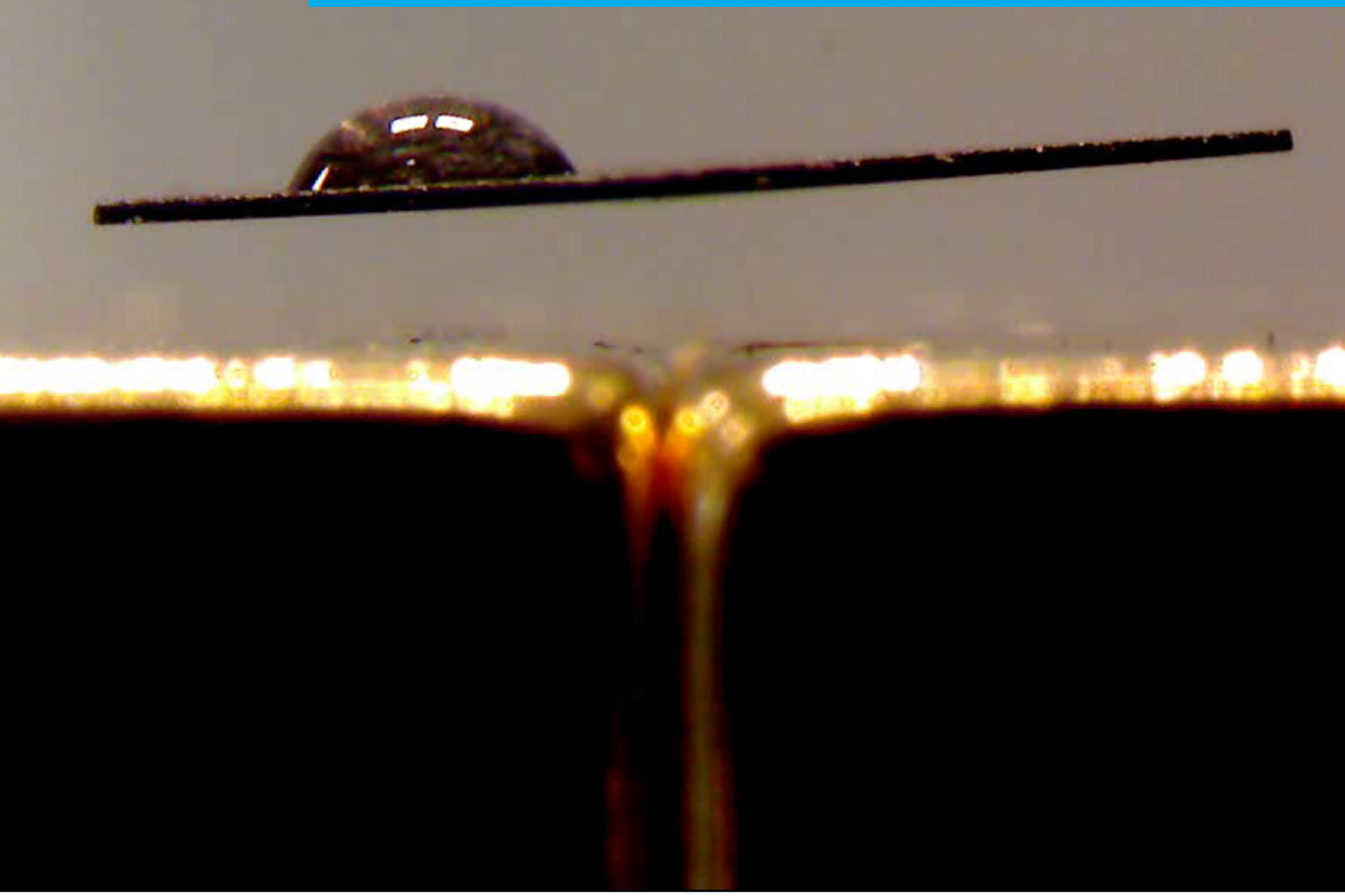

TU Delft Delft University of Technology

Challenge the future

Diamagnetically Levitated Resonant Mass Sensor

Master of Science Thesis

For the degree of Master of Science in High Tech Engineering at Delft University of Technology

Nimit Kothari

26 July, 2019

Student Number:	4737547	
Project Duration:	November 1, 2018 - July 26, 2019	
Thesis committee:	Prof. dr. P. G. Steeneken,	Delft University of Technology
	Dr. F. Alijani,	Delft University of Technology
	Dr. M. K. Ghatkesar,	Delft University of Technology
	Dr.ir. S. Vollebregt	Delft University of Technology

Faculty of Mechanical, Maritime and Materials Engineering (3mE) ·
Delft University of Technology

Abstract

In the past few decades, there has been a growing demand for low-cost disposable sensors to be utilized in hazardous and toxic environments such as high temperature and chemically aggressive environments, which can lead to irreversible damage to the sensor. Moreover, by cost reduction, they become more attractive for utilization in developing countries, where the research of new biomedical technologies has been restricted due to a decentralized healthcare system, lack of infrastructure and shortage of investment.

This research focuses on developing a low-cost, disposable and easy to use mass sensor utilizing diamagnetic levitation. Diamagnetic levitation is the only stable form of levitation at room temperature and does not require external sources of energy, feedback loops or cooling for stable levitation. It is a low cost, easy to use, disposable sensor that makes it suitable for potential point-of-care applications. The sensor consists of a pyrolytic graphite plate that levitates above a checkerboard arrangement of permanent magnets with alternating magnetization. The system is actuated using electromagnetic excitation and the material properties of the sample are extracted by conducting a multimodal analysis of the resonance frequencies and mode shapes; measured using a laser Doppler vibrometer (LDV). An opto-electronic phase lock loop utilizing the LDV is used to bring the levitating pyrolytic graphite into sustained mechanical oscillation controlled by a PID controller. The experimental mass sensitivity is measured by analysing the frequency shift associated with the placement of glass beads. The frequency stability is measured by computing the Allan deviation and the experimental precision of mass sensor is then computed. The results show that the precision of a diamagnetically levitated resonant mass sensors decreases with the decrease of the size of the levitating oscillator. The precision of a levitating oscillator of side length 2 mm and thickness 0.08 mm is found to be 14.4 pg at a gate time of 0.1 s for an instantaneous change in frequency.

Table of Contents

Acknowledgment

It has been nine months since the beginning of this project, although it feels much shorter. The whole project has been a wonderful experience, teaching me that there is always something new to learn every day. Reaching the end of the project, I would like to thank everyone who has made it possible in one way or the another. Firstly, I would like to express my profound gratitude and regards to my supervisor, Peter Steeneken for giving me an opportunity to work on the project and continuous guidance not just throughout the course of the project, but also as a mentor during my master's programme at TU Delft. Along with Peter Steeneken, I would also like to thank Farbod Alijani for the multiple coding and brainstorming sessions, regular feedback and recommendations as well as showing how to face both difficult and joyful situations in life.

I would be amiss if I don't mention Ata's continuous help and advice since even before the beginning and throughout the project. I would also like to thank Tomas, Irek, Vincent and Xianfeng for their help whenever it was needed. I would pay special thanks to my friends, Bhavya and Arun for their constant support throughout the course.

Finally, and most importantly, I will thank my parents and brother for their wholehearted support and constant encouragement, without which I would not have been where I am today.

Nimit Kothari
26 July, 2019

Chapter 1

Introduction

The emergence of levitation has attracted widespread interest leading to numerous applications ranging from bullet trains to levitating magnetic bearings. Levitation in simple terms can be described as free flotation of solid or liquid matter. The major obstacle in the physics of levitation was not the lack of contact free forces but the stability of levitating objects. With advancements in technology, various forms of stable levitation became possible. Different types of stable levitation include aerodynamic, acoustic, optical, electrical, radio-frequency and magnetic levitation[1]

Magnetic levitation has emerged at the forefront of levitation technologies as reviewed by Yaghoubi[2]. The current usage of magnetic levitation across the different spectra of applications include and are not limited to electromagnetic suspension, electrodynamic suspension, maglev trains, linear motors, launching rockets, fans and heart pumps. Trains based on magnetic levitation primarily use Electromagnetic suspension (EMS) and/or Electrodynamic Suspension for levitation. While EMS is inherently unstable and requires an active control to maintain the air gap between the guideway and electromagnets, EDS needs sufficient speed to generate eddy currents for stable levitation[3].

Passive stable magnetic levitation can be achieved only with superconductors and diamagnetic materials [1]. Levitation using superconductors has been shown to have applications for high speed bearings and ground transportation. Levitation using superconductors requires certain metals and alloys to reach a temperature close to 0 K to achieve a state with zero resistance known as the Meissner state and thus requires energy input for stable levitation at room conditions[4]. Compared to the superconductor based magnetic levitation, diamagnetic levitation requires permanent magnets and a diamagnetic material for completely passive stable levitation mechanism requiring no external energy input at room conditions. Hence, diamagnetic levitation currently remains the simplest mechanism in principle to achieve stable levitation[5]. Diamagnetic levitation benefits from scale reduction and it is theorized that it can be achieved for any known material if the dimensions were reduced adequately[5]. Hence, diamagnetic levitation has wide-ranging applications at the micro and nanoscales. This work aims to utilize diamagnetic levitation to build a levitating oscillator to be utilized as a mass sensor.

1-1 Thesis Outline

The second chapter covers the state of the art in diamagnetic levitation and its applications. It also provides a brief overview of the currently prevalent mass sensing techniques in MEMS technologies and formulates the research gaps based on the conducted survey. The third chapter provides the motivation and the research question to be investigated in this thesis and presents the methodology to be followed for the investigation. The fourth chapter presents the dynamical analysis and sensitivity analysis conducted in this thesis in the form of a paper followed by conclusions and recommendations in the next chapters. A brief reflection of the whole research project along with a future outlook of the author is presented at the end.

Chapter 2

Literature Review

This chapter aims to give the reader a brief introduction in the field of diamagnetic levitation. Firstly, the discovery and explanation behind diamagnetism in matter is provided. The stability analysis and experimental demonstrations of diamagnetic levitation is then covered briefly, proceeding with an in-depth analysis of the state of the art in utilization of diamagnetic levitation in varying applications. A brief overview of the current mass sensing technologies and their limitations is followed by conclusions and research gap identification.

2-1 Diamagnetism

Matter can be broadly classified into three principal classes based on their magnetic properties: 1. Ferromagnetic 2. Paramagnetic and 3. Diamagnetic. Ferromagnetic materials can have a magnetic moment in the absence of an external magnetic field and are used as permanent magnets. Paramagnetic and diamagnetic materials develop an induced magnetic moment on the application of an external magnetic field in the positive and negative direction respectively[6].

Diamagnetism is present in all matter but is much weaker than the other two classes and gets subsided in their presence. Hence, materials where only the diamagnetic effect is present, are termed as diamagnetic materials[7]. Diamagnetism was first discovered by Dutch philosopher Anton Brugmans in 1778 when he observed that a piece of hanging bismuth ball moves away in the presence of a powerful electromagnet. Faraday analysed the rotation of polarised light under the influence of magnetic field and proved that magnetism was a universal property of matter. After investigating the movement of suspended materials like glass from the poles of powerful electromagnets, he announced the discovery of a very weak magnetic property of matter on 4 November 1845. The repulsion of these materials from the magnetic field was similar to weak electrostatic repulsion; hence he termed these materials 'diamagnetics' as compared to its electrical counterpart dielectric[8].

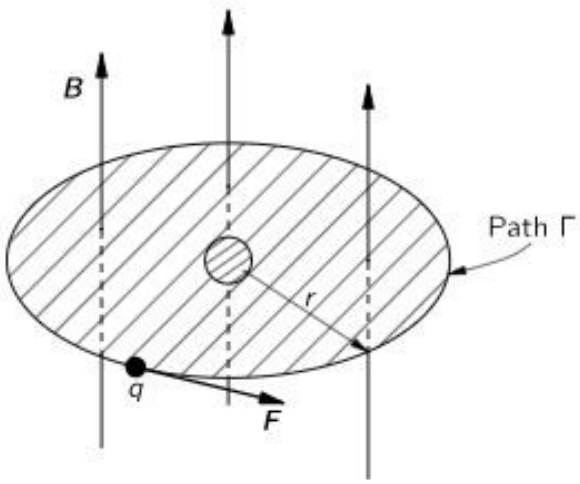

Figure 2-1: Analysing the change in magnetic moment of a charged particle with charge 'q' and mass 'm' revolving around the nucleus at a fixed distance 'r' with change in externally applied magnetic field[7]

The mechanism of diamagnetism is a purely quantum phenomenon but many textbooks for the sake of simplicity work out a classical explanation. The most common classical explanation is to analyse the change in the magnetic moment of a charged particle revolving around the nucleus at a fixed distance 'r' as shown in Figure 2-1. The application of an external magnetic field leads to an induced electromotive force(emf). The induced emf produces a torque on the revolving charged particle thereby leading to a change in the angular momentum of the particle and consequently on the magnetic moment of the charged particle. This change in the magnetic moment of the charged particle has an opposite direction to the applied magnetic field as per Lenz law and therefore leading to diamagnetism[7].

The actual explanation of the mechanism of diamagnetism requires delving into the realm of quantum mechanics in its full glory. However, there are some researchers who favour a semi-classical explanation of diamagnetism which is skipped in here for the sake of brevity and the reader is referred to the article by O'Dell and Zia for detailed explanation[9]. Since the work in this thesis will be on micro-scale, the approximate classical understanding of diamagnetism will be adequate for grasping the physics of the phenomenon.

2-2 Diamagnetic Levitation

Earnshaw played a major part in analysing the stability of levitation using magnetic and electrostatic forces. Earnshaw proved that a test particle in the presence of a curl-free and or divergence-free field will not have a stable equilibrium in any configuration[10]. Earnshaw discovered that electrostatic and magnetism forces are proportional to $1/r^2$. Hence, there would be no stable minima possible for a static condition (force equilibrium) and result in a saddle point[11].

However, Earnshaw was not aware of the existence of diamagnetic materials and did not take them into account. After the discovery of diamagnetism by Faraday in 1845[12], William

Thomson developed the mathematical background for the diamagnetic materials; showcasing that their behaviour under the influence of an external magnetic field is similar to paramagnetic materials but with a negative sign. With the help of this analysis, Thomson proposed the possibility of stable diamagnetic levitation[8]. Braunbek was the first one to experimentally show that stable diamagnetic levitation was in fact possible. He experimentally showed that bismuth and graphite can be levitated with the use of electromagnets[13].

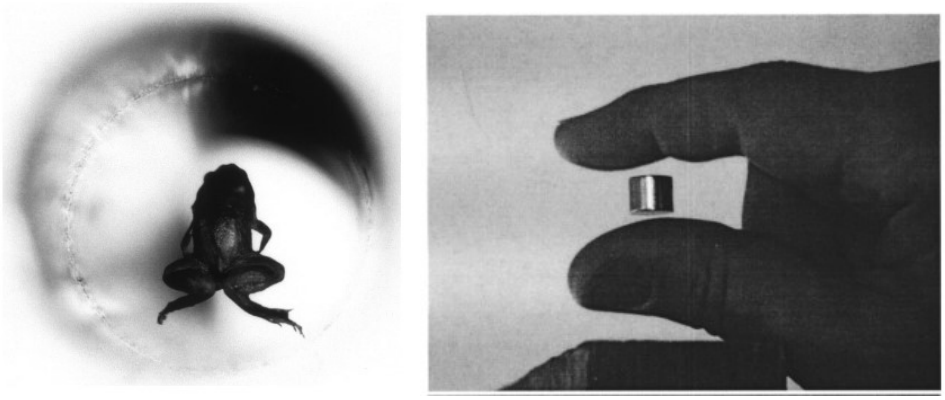

(a) **(b)**

Figure 2-2: a) Levitation of a frog inside a powerful solenoid shown on the left. b) The levitation of a magnet stabilized using the diamagnetism of human fingers in the lab at Nijmegen[11]

Major recent advances were orchestrated by Simon, Heflinger and Geim[14][15][11]; where they levitated a frog in a stable zone of a 16T magnet. They also levitated a magnet below a superconducting solenoid; stabilising it using the diamagnetism of fingers in their lab at Nijmegen. Geim showed that it is possible to levitate human beings with a 40T racetrack magnet[16], but proposed it for the future and left levitation of human beings to more conventional methods such as helicopters for the time being. Their work was pioneering in the field of diamagnetic levitation and the research interest in the field has ramped up ever since. The historical development of diamagnetic levitation with the major milestones can be summarized as shown in Figure 2-3.

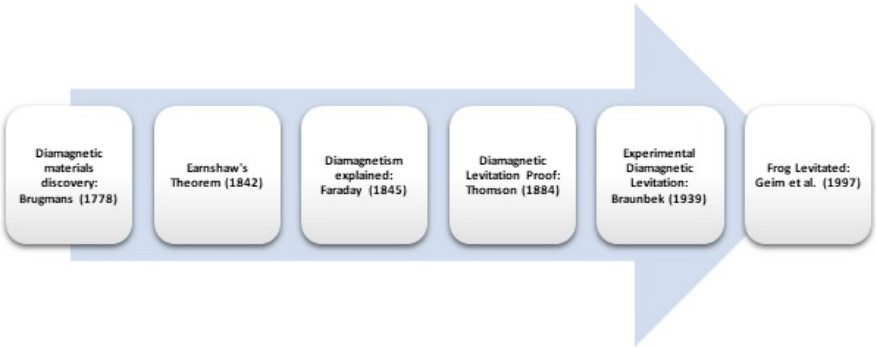

Figure 2-3: A brief summary of the milestones in the discovery and development of diamagnetic levitation

2-3 State of the art

The utilization of diamagnetic levitation has been primarily focused on developing various sensors and actuators. Since diamagnetism is a weak force, its utilization in the macro scale proves difficult. Diamagnetic levitation benefits from scale reduction laws as the force to volume ratio for interaction between magnet and diamagnetic material are increased by a length factor on scale reduction. This is owing to the fact that magnetic field gradient gets multiplied by a length factor when the distances are scaled down by the same as the diamagnetic force is directly proportional to the field gradient[17]. It can be used as an explanation for the fact that most of the applications developed utilizing diamagnetic levitation work in the micro-scale.

2-3-1 Early Applications

After the experimental proof of concept by Braunbek, Waldron et al.[18] developed a bearing by levitating a flat ring of pyrolytic graphite with a mass of 0.933 g over the circular gap of permanent magnets. They analysed the dynamic behaviour of this setup by exciting it using ultrasound waves to obtain the rigid body resonances and extract the stiffness information. The bearing was accelerated using a capillary air bleed in a vacuum bell jar to analyse its dynamic losses; and it was observed that the efficiency of momentum transfer was about 8 percent.

Simon et al[19] developed a tiltmeter by levitating a cylindrical diamagnetic seismic mass between a predefined magnetic configuration to obtain a weakly constrained motion in one direction while being strongly constrained in the other direction as shown in Figure 2-4. A sleeve of aluminium was put on the seismic mass to damp the vibrations for quick real time output. A photodiode was used to measure the displacement of the seismic mass. The setup was taken 600 m underground and was able to detect the periodic tidal wave motions along with major seismic activities such as earthquakes and storms.

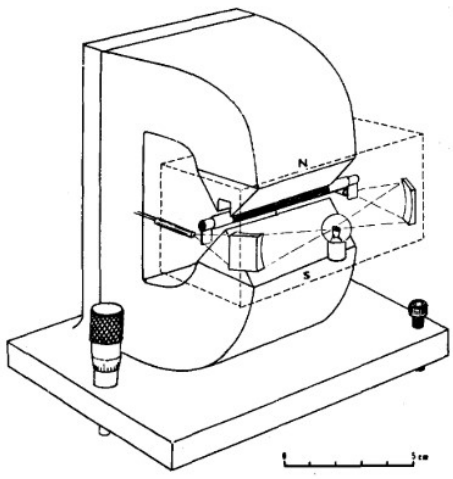

Figure 2-4: Diamagnetic Levitation based tiltmeter with a photodiode as a displacement sensor to measure seismic activity[19]

2-3-2 Liquid Levitation

The development in the field of diamagnetic levitation was not restricted to only levitation of solids. Beaugnon and Tournier[20] showed that it is also possible to levitate liquids as well. A hybrid magnet with field up to 27T was used to levitate liquid in glass tubes. Glass tubes filled with water/alcohol/acetone were lowered in the magnetic field of the magnet and the change in their level was detected. Beaugnon et al.[21] in their further work levitated an ethanol droplet of size 6mm in vertical solenoid's magnetic field. The dynamic behaviour of the levitated droplet was studied by exciting it using two air nozzles positioned at opposite ends and read out using a CCD camera to evaluate its surface tension properties assuming the droplet to be spherical as shown in Figure 2-5. These experiments concur with the results obtained from microgravity expectations and opened diamagnetic levitation to a new range of applications.

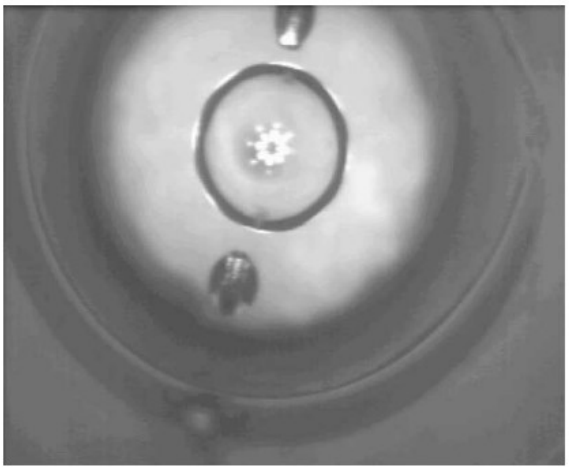

Figure 2-5: Levitation of 6mm ethanol droplet. The levitated droplet is excited in its resonant mode to evaluate the surface tension based on the frequency response[21]

2-3-3 Microgravity

Geim and Tisha [22] utilized diamagnetic levitation to simulate microgravity to detect earth's rotations. A spinning sphere is levitated inside a bitter magnet and spun by means of airflow with 20Hz. The rotor precession was manually readout with a telescopic lens and achieved accuracy equivalent to military and quantum gyroscopes at the time. Their basic system left room for major improvements with precise readout, better machining of rotor and combination with a superconducting magnet. This research led to more utilization of diamagnetic levitation for generating microgravity/low-gravity conditions. Brooks and Cothern [23] leveraged this characteristic to analyse the dynamics of single and multiple granular particles. A stable levitation zone was created inside a bitter magnet and the dynamic behaviour of single and multiple particles with varying field intensity and density to susceptibility ratio was readout by a video camera. This setup provides a unique method to analyse the deterministic and chaotic motion of granular particles.

2-3-4 Micromanipulation

The second biggest field utilizing diamagnetic levitation is the micromanipulation-based actuation of levitated objects. Positioning stages and actuation based on magnetic levitation technologies are very common in the current world due to its non-contact nature. The usage of magnetic levitation technology in micro and nano-positioning systems is very advantageous as it eliminates effects such as friction, backlash, stiction and hysteresis present in traditional mechanical systems [24]. Combined with the capability to be completely passive and ability to levitate liquids as well makes diamagnetic levitation a more efficient solution for micromanipulation systems.

The utilisation of magnets levitated over diamagnetic materials as microbots was first presented by Pelrine [25] and further experimentally shown in his later work [26]. The assembly of magnets in opposite neighbouring pole configuration levitates above a sheet of pyrolytic graphite. Traces of printed circuit boards are used to drive the system in feedforward as they are devoid of friction and other restricting mechanical effects. They demonstrated open loop repeatability of 200nm and developed a zone-based control for a swarm of microbots.

Kobayashi and Abe [27] on the other hand levitated a pyrolytic graphite disc, which was actuated optically by varying the local magnetic susceptibility of the disc by heating it using a laser source and work as a microbot and a rotor. Kang et al.[28] used the thermo-optical coupling to generate photo-gated motion of the levitating graphite on an array of magnets with a gradually decaying magnetic field configuration. While the microbot actuated using the printed circuit board provided precise movement, the thermo-optical coupling-based actuation still needs to prove its accuracy and feasibility.

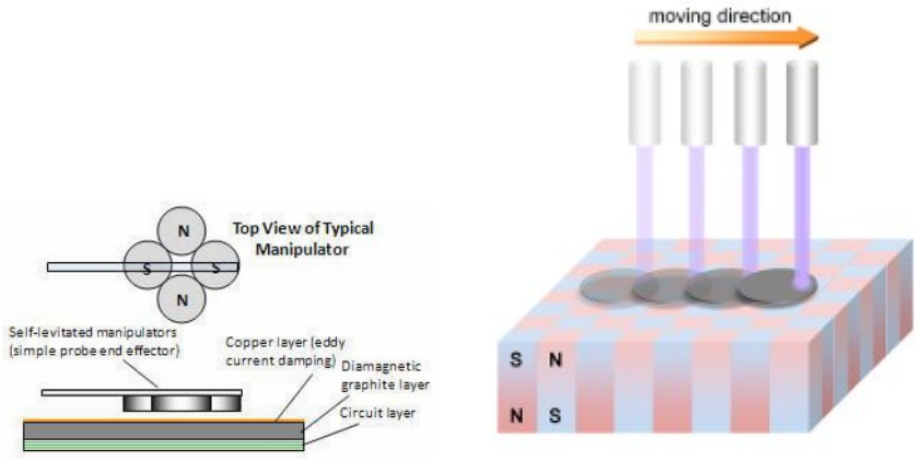

Figure 2-6: a) Diamagnetically levitated magnet stabilized by graphite sheet and actuated by layers of printed circuit board traces[26]. b) Optically actuated graphite disc levitating over permanent magnet array[27].

The manipulation and positioning systems employing diamagnetic levitation were not restricted to solid levitation only. Lyuksyutov et al. [29] experimentally levitated femtodroplets of water and glycerine utilising micron scale permanent magnets to develop a micro-

manipulation chip (MMC). The 23 µm diameter glycerine and water droplets were levitated in a slit between two permanent magnets and manipulated with electrodes inserted in the slit. Chetouani et al. [30] deposited microarrays of magnets on silicon substrate to build magnetic traps for droplets and latex beads. Water, ethanol, oil and glycerine droplets were shown to move along the grooves after dispensing by a piezoelectric dispenser as shown in Figure 2-7.

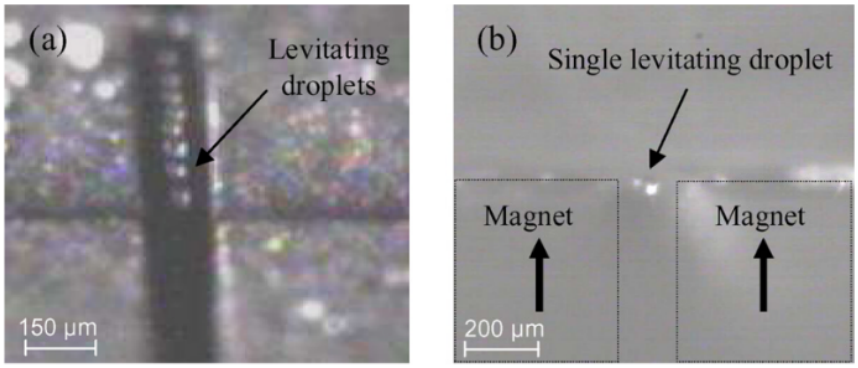

Figure 2-7: a) Array of levitated water droplets levitated in a slit between formed two magnets b) Magnetic configuration showcasing levitation of a single $30\,\mu\mathrm{m}$ droplet[30].

2-3-5 Rotor Systems

Developments in utilization of diamagnetic levitation as actuator led to increased research in the usage of such systems as bearings and rotors. Cansiz and Hull [31] used a disc shaped permanent magnet as rotor levitated by ferrite ring magnet and stabilised by bismuth plates. The steady state analysis showed that the rotor will not be feasible for large loads but for small scale applications. The dynamic losses of the rotor were computed by actuating it using a cold gaseous nitrogen jet and were found to be predominantly due to eddy currents and dependent on the frequency of rotation. This was also observed in his future work to analyse the resonance of the system in vertical, radial and tilt directions [32].

Liu et al. [33] used a gear shaped pyrolytic graphite disc levitated over cylindrical permanent magnets as the rotor for unconstrained rotation around the z axis. This microrotor system was actuated using three phase axial variable capacitance principle. The stator situated on top of the magnets has a 12 pole driving electrode in comparison to the rotor's 8 driving poles as seen in Figure 2-8. The efficiency of the system was quite low as a 30V input led to 10rpm output. Su et al. [34] meanwhile applied gas flow to actuate the rotor achieving a maximum speed of 500rpm for an input flow rate of 28sccm. Xu et al. [35] attached a sheet of glass on top of the rotor to help in its electrostatic actuation and achieved a maximum speed of 140rpm.

2-3-6 Inertial Systems

Barrot et al. [36] used a pyrolytic graphite disc levitating over checkerboard configuration of magnets to act as a 2D acceleration sensor. An aluminium ring surrounding the diamagnetic disc acting as reflectors for optical sensor measurement was proposed for the accelerometer.

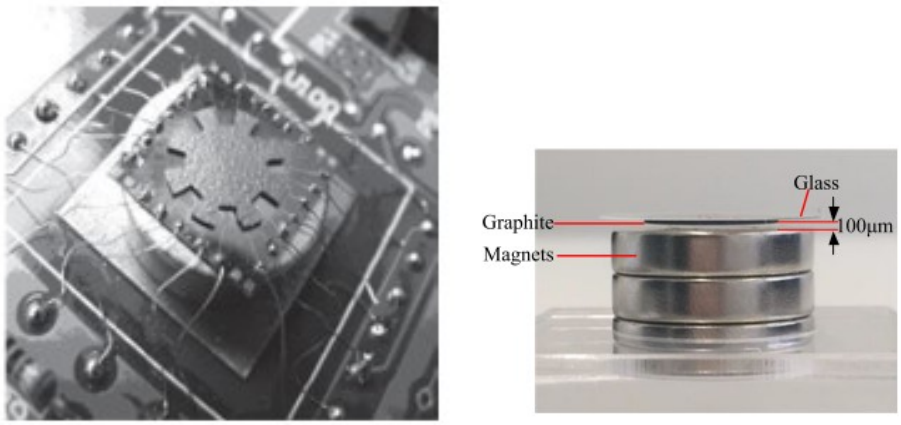

(a) (b)

Figure 2-8: a) The three phase variable capacitance based microrotor shown here has the driving electrodes situated at the stator with the levitating pyrolytic graphite as the rotor[33]. b) The microrotor shown here has a glass plate attached to the levitating rotor[35].

Garmire et al. [37] mounted a silicon on insulator proof mass; whose movements were sensed using a finger comb based capacitor and also an interferometer. They respectively achieved sensitivity of 34 µg and 6 µg. Pasquale et al. [38] proposed that diamagnetic levitated systems can be used as energy harvesters by comparing the stiffness of levitated accelerometer with mechanically suspended accelerometers. Energy harvesters based on diamagnetic levitation have been on the rise since.

Liu and Yuan [39] proposed utilizing a magnet levitated with the help of lifter magnet and stabilized by spiral diamagnetic coils to be utilized as an energy harvester. The spiral coil was proposed to reduce the eddy current losses present in the system. However, they could not fabricate bismuth coils, and hence used copper coils for energy transduction and pyrolytic graphite for diamagnetic stability; but did not achieve enough levitation gap to reach non-linear regime. Palagummi and Yuan [40] optimized the design of a similar system by parametrizing the geometrical and aspect ratios of the floating magnet and diamagnetic plate to maximize the force between them. The eddy current losses were reduced by cutting the graphite in two pieces of 2 mm and then joining them with an insulator in between. Their first design achieved an efficiency of 1.54 percent; which is shown in Figure 2-9. They made a similar system which was levitated horizontally and achieved an efficiency of 2.5 percent. Clara et al 2016 [41] also propose a viscosity and density sensor using diamagnetic levitation, wherein the resonant rotary oscillations of levitated spherical neodymium floater magnet. A hall sensor is used to measure the levitation height. Actuated using Helmholtz coils in the x and y direction, the coil in the z direction is used to readout the oscillations.

2-3-7 Force and Mass Sensing

Boukall, Piat and Abadie[42] first laid the theoretical foundations for developing a micro-nano force sensor utilizing passive diamagnetic levitation. They developed a prototype of the suspension mechanism consisting of eight cube magnets to provide lifting force to suspended cylindrical magnets stabilized by diamagnetic plates in the horizontal direction. The

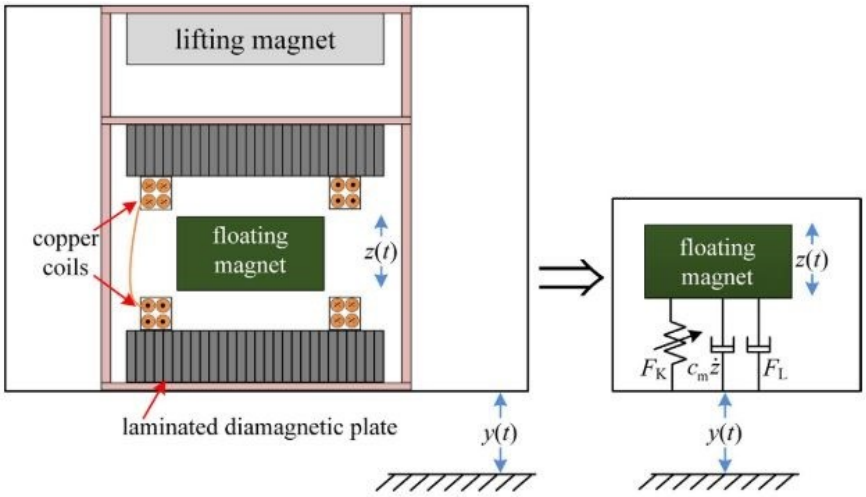

Figure 2-9: Setup for vertical diamagnetic levitation (VDL) based energy harvester. The diamagnetic plate is laminated to reduce eddy current losses. the system is modelled as 1-DoF spring-mass damper system[40].

displacement of the sensor to an applied force is measured using a laser sensor and a linear response is obtained with a sensitivity of $19\,\mathrm{nN\,\mu m^{-1}}$. Li, Kim and Rydberg [43] utilized a diamagnetically levitated graphite plate to calibrate the lateral force constant of AFM tips. In recent past, Keskekler [44] accurately modelled the rigid body dynamics of diamagnetically levitated graphite plates along with analysing the effect of trapped charges on the dynamics of levitated plates. His work also investigated a new phenomenon of impact oscillator with electrostatic actuation of the levitated plate.

Pelrine et al.[26] developed a mass sensor using the DM3 microbot. A weighing pan as shown in Figure 2-10 was attached on top of the levitating magnets and the deviation in the trajectory due to an added salt crystal was evaluated to calculate the mass sensitivity. The reported mass resolution utilizing the weighing pan mechanism leveraging DM3 robot was reported to be $10\,\mu g$.

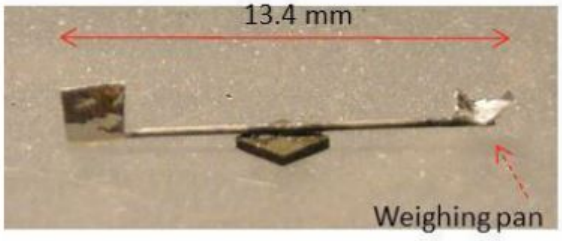

Figure 2-10: Weighing pan attached on top of DM3 robot comprising of magnets with alternating magnetization to be utilized as a weighing pan by measuring the change in trajectory of the robot associated with an added mass[26].

2-3-8 Mass Sensors: Overview

The most promising approach for mass measurement in micro and nano systems currently are clamped cantilever based mechanical resonators [45]. The most prevalent measurement system analyses the dynamic behaviour of clamped cantilever beams. The added mass at the tip of a cantilever beam clamped at the other end leads to a decrease in the frequency. Such a shift is attributed to the increased kinetic energy of the system. However, the stiffness of the added mass counteracts the kinetic energy effect. The geometrical position along the mass and size and shape of the adsorbate was simultaneously measured by Hanay et al. [46], while Ramos et al.[47] varied the position of the adsorbate to measure the mass and stiffness at the nodes and anti-nodes of the bending modes. The utilization of cantilever based resonators always requires a clamped plate which can introduce prestresses in the system leading to inaccurate measurements. As reported by Hauzer [45]; the clamping of cantilever chip introduces clamping induced damping and affects the resonance frequencies. The process of fabrication of nano-structure requires the chip to be taken out and re-positioned in the clamp for measurements and can lead to internal stresses as well. The fabrication and manufacturing costs also act as hindrances for the utilization of cantilever based resonators.

Another prominent field of mass sensor utilizes acoustic waves based resonators. The two main types of acoustic wave based resonators are bulk acoustic wave (BAW) and surface acoustic wave (SAW) based resonator[48]. However, the acoustic wave based resonators are "low temperature" technology[49], and suffer many problems when operated at high temperature ranges[50]. The most recent advancement in the field of mass sensing involves utilizing carbon nanotubes for yoctogram measurement[51]. The challenges in using these technologies lies in the requirement of complicated infrastructure and extreme conditions such as ultrahigh vacuum environments.

2-4 Conclusion

The existing and expected improvements in the development of micromagnets[17] and material fabrication techniques[52] make diamagnetic levitation a critical proponent for a range of suspended sensors and actuators in the microscale. The ability of diamagnetism to simulate gravity free environments provides it with tremendous potential for future space-based and biological applications. With the possibility to levitate in water and other liquids opens a plethora of applications ranging from studying the rate of chemical and biological reactions to lab on chip applications. There have been several MEMS sensors and actuators developed based on the rigid body motion of diamagnetically levitated objects which has been studied in detail. However, the study of flexural dynamics of levitated objects can be identified as a research gap based on the conducted survey. Hence, this thesis focuses on analysing the flexural vibrations of diamagnetically levitated objects and utilize it to develop an oscillator for mass sensing.

Chapter 3

Research Question and Methodology

In the past few decades, there has been a growing demand for low cost disposable sensors to be utilized in hazardous and toxic environments such as high temperature and chemically aggressive environments, which can lead to irreversible damage to the sensor. Moreover, by cost reduction, they become more attractive for utilization in developing countries, where the research of new biomedical technologies has been restricted due to a decentralized healthcare system, lack of infrastructure and shortage of investment [53].

This research focuses on developing a low cost, disposable and easy to use mass sensor utilizing diamagnetic levitation. Diamagnetic levitation is the only stable form of levitation at room temperature and does not require external sources of energy, feedback loops or cooling for stable levitation[1]. Stable levitation also eliminates unwanted mechanical effects such as mechanical cross talk among arrays of oscillators and clamping induced damping[45] affecting MEMS devices. The levitating proof mass provides physical decoupling between the sensing element and the electronic components making the sensor suitable for harsh environments such as high temperature ranges compared to acoustic wave based resonators[50]. This contact-less nature also allows the levitating proof mass to be utilized as a disposable element for usage in irreversible processes.

As presented in the previous chapter, there has been tremendous development of applications utilizing diamagnetic levitation in recent time with detailed study of its rigid body modes. However, the study of flexural vibrations of diamagnetically levitated objects has not been conducted and remains a research gap. Hence, the objective of this study is to analyse and build a diamagnetically levitated oscillator for mass sensing in air utilizing its flexural vibrations. The research question to be answered is then formulated as:

What is the precision of a diamagnetically levitated resonant mass sensor in air?

3-1 Research Methodology

This thesis focuses on analysing the flexural vibrations of diamagnetically levitated objects. Hence, the first step is to develop an actuation and measurement setup to obtain the flexural resonance frequencies and mode shapes. The theoretical modelling of the flexural vibrations needs to be performed for further analysis. The second step is to obtain the effective modal mass of the resonator experimentally. The final step is to develop a phase lock loop for the analysis of frequency stability of the oscillator and estimate the precision of the mass sensor.

Chapter 4

Sensitivity of diamagnetically levitated resonant mass sensor

Sensitivity of diamagnetically levitated resonant mass sensors

Nimit Kothari,[1] Ata Keşkekler,[1] Farbod Alijani,[1, a)] and Peter G Steeneken[1, 2, b)]
[1)]*Department of Precision and Microsystem Engineering, Delft University of Technology. 2628CD Delft, The Netherlands*
[2)]*Kavli Institute of Nanoscience, Delft University of Technology, 2628CJ Delft, The Netherlands*

(Dated: 22 July 2019)

This article presents an oscillating mass sensor under stable levitation using diamagnetic forces. The sensor consists of pyrolytic graphite plate that levitates above a checkerboard arrangement of permanent magnets with alternating magnetization. The system is actuated using electromagnetic excitation and the material properties of the sample are extracted by conducting a multimodal analysis of the resonance frequencies and mode shapes; measured using a laser Doppler vibrometer (LDV). An optoelectronic phase lock loop utilizing the LDV is used to bring the levitating pyrolytic graphite into sustained mechanical oscillation controlled by a PID controller. The frequency stability is measured by computing the Allan deviation and the experimental mass sensitivity is extracted by analysing the frequency shift associated with glass beads. The results show that the experimental precision of a diamagnetically levitated resonant mass sensor depends on the dimensions of the oscillator. The precision of a square plate of side length 2 mm and thickness 0.08 mm is found to be 14.4 pg at a gate time of 0.1 s for an instantaneous change in frequency.

In the past few decades, there has been a growing demand for low cost disposable sensors to be utilized in hazardous and toxic environments which can lead to irreversible damage to the sensor[1]. Moreover, by cost reduction, they become more attractive for utilization in developing countries, where the research of new biomedical technologies has been restricted due to a decentralized healthcare system, lack of infrastructure and shortage of investment[2]. Hence, there is an urgent need to develop feasible, portable, low cost and easy to use point-of-care sensors[3].

This article focuses on developing a low cost, disposable and easy to use mass sensor utilizing diamagnetic levitation. Diamagnetic levitation is the only stable form of levitation at room temperature and does not require external sources of energy, feedback loops or cooling for stable levitation[4]. It's low cost, easy to use and disposable nature makes it a suitable technology for point-of-care applications. Stable levitation also eliminates unwanted mechanical effects such as mechanical cross talk among arrays of oscillators and clamping induced damping[5] affecting MEMS devices. The levitating proof mass provides physical decoupling between the sensing element and the electronic components making the sensor suitable for harsh environments such as high temperature ranges[6]. This contact-less nature also allows the levitating proof mass to be utilized as a disposable element for usage in irreversible processes.

Diamagnetic levitation has piqued interest in recent times after the demonstration of a levitating frog inside a 16T magnet and a magnet levitating between two fingers by Berry and Geim[7], Simon and Geim[8] and Geim et al.[9]. A new generation of energy harvesters have been developed by employing levitating magnet(s) as proof masses in mono-stable and bi-stable configuration as well as horizontal and vertical configuration by Palagummi and Yuan[10–12]. Chetouani et al.[13,14] demonstrated the levitation of bismuth in air and copper and silicon in paramagnetic liquid over rails of NdFeB magnets; sputtered over grooves etched on a silicon wafer. The levitation of water microdroplets and latex in air and paramagnetic liquid respectively on micromachined NdFeB bulk magnets was also achieved. Clara et al.[15] developed a viscosity and density sensor using diamagnetic levitation, wherein a levitating spherical neodymium floater magnet is excited in its rotational oscillation mode and the shift in resonance frequency and quality factor enables the extraction of the viscosity and density of the liquid. Pelrine et al.[16] developed a microbot by levitating checkerboard arrangement of magnets over a pyrolytic graphite sheet on top of a printed circuit board; controlled using varying magnetic fields by varying the currents in the printed circuit board. The microbot was utilized to act as a mass sensor by measuring the change in trajectory by the placement of a mass on a weighing pan attached to it. The mass sensor achieved a resolution of 10 µg. Further, there has been development of accelerometer[17], gyroscope[18], force sensors[19], impact oscillators[20], bearings[21], and tiltmeter[22] leveraging diamagnetic levitation.

In our experiments, a square plate of pyrolytic graphite is levitating over a checkerboard arrangement of magnets with alternating magnetization. Square pyrolytic graphite plate of different sizes is developed for this study by first cleaving and polishing the pyrolytic graphite sample, followed by laser cutting. An electromagnetic coil is used to actuate the levitating plate and obtain the flexural modes and resonance frequencies of the plates. The first three flexural resonance frequencies and mode shapes obtained for the square plate of side length 4 mm observed using laser Doppler vibrometer (LDV) are shown in Fig 1a. The resonance frequencies of the plate for multiple levitation configurations is obtained (SI). It is found that the change in the resonance frequencies of the plate with the changing magnetic flux density is negligible. Hence, the levitating plate can be modelled as a free plate[23].

[a)]Electronic mail: f.alijani@tudelft.nl
[b)]Electronic mail: p.g.steeneken@tudelft.nl

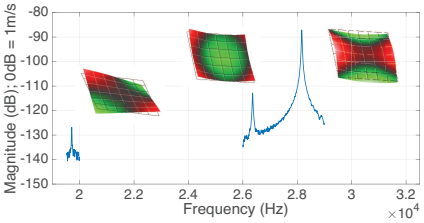

(a)

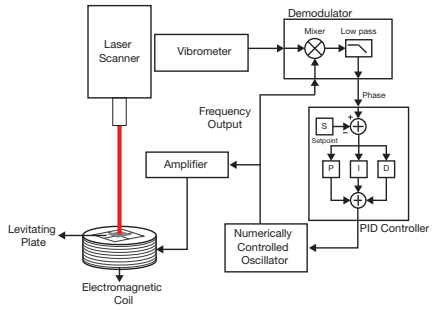

(b)

FIG. 1: **a)** The first three flexural modes of a square plate of side length 4 mm and thickness 100 µm levitating on 4x4 parallel magnetic configuration, actuated using an electromagnetic coil and read out using a laser Doppler vibrometer (LDV). **b)** The schematic of the experimental setup used for developing a diamagnetically levitated oscillator. The voltage readout from the LDV is fed into the lock-in amplifier which uses PID control for phase set-point tracking. The numerically controlled oscillator (NCO) controlled by the PID controller drives the electromagnetic coil for sustained oscillation. The picture of actual experimental setup can be found in SII.

The dynamical behaviour of the flexural vibrations of levitating rectangular pyrolytic graphite plate has been modelled using Rayleigh Ritz and Finite Element method. The Rayleigh Ritz method and Finite Element model are then utilized to extract the Young's modulus (E) and the in plane Poisson's ratio (ν_{xy}) by minimizing the root mean square error between theoretically (Rayleigh Ritz and FEM) and experimentally obtained frequencies using a gradient search optimization algorithm. The detailed convergence analysis and results are presented in SI. The material values obtained are $E = 39.3\,\text{GPa}$ and $\nu_{xy} = -0.212$; which are in close approximation with the values obtained by Bert[24]. Pyrolytic graphite is fabricated by the deposition of layers of wrinkled and wavelike hydrocarbons at high temperatures[25]. These wrinkled layers of pyrolytic graphite can explain the in-plane negative Poisson's ratio as observed similarly in graphene membranes[26,27]. The density of the plate is experimentally measured to be $2260\,\text{kg m}^{-3}$. The detailed dynamical analysis as briefly described above is presented in SI.

After the characterization of the dynamics of levitated plate, the next step is to understand the mass sensitivity of the plate. The frequency shift $(\delta\omega)$ of a resonator due to an added mass (δm) is defined as :

$$\delta\omega = -\frac{1}{2}\frac{\omega}{M_{eff}}\delta m \tag{1}$$

Here $\Re = -\frac{1}{2}\frac{\omega}{M_{eff}}$ is defined as the mass sensitivity of the resonator. where M_{eff} is the effective modal mass. Rayleigh Ritz method and Finite Element model are utilized to obtain the theoretical effective modal mass $(M_{eff,th})$. The detailed explanation of the procedure to obtain $(M_{eff,th})$ is provided in SI.

The effective modal mass obtained from Rayleigh Ritz model and the Finite Element Model are the same and are termed as $M_{eff,th}$. The experimental verification of the M_{eff} is performed by conducting two sets of experiments. Firstly, frequency shift associated with placement of glass beads of diameter 75 µm at the anti-node of the third flexural mode on levitating square plates of side length 2 mm, 3 mm and 4 mm was measured as shown in Figure 2a. The glass beads were picked manually by utilizing the capillary forces of a water droplet. A water bead attached to a syringe was used to pick up the glass beads from the petri dish, and then the water bead containing the glass bead was deposited manually on the stationary pyrolytic graphite plate. The detailed frequencies obtained with and without the bead are presented in SII.

The second set of experiments analysed the evaporation rate of a water droplet. The evolution of third flexural resonance frequency and quality factor with the evaporation of a water droplet was measured by conducting continuous sweeps using a vector network analyser (VNA). The water droplet with fixed volume was dispensed using an Eppendorf precision pipette. The evolution of the resonance frequency and quality factor for the evaporation of 0.55 µl of deionized water is shown in Figure 2b. The evaporation of the water droplet was also recorded using a digital microscope to analyse the evaporation rate of the water by measuring the contact angle and height of the droplet.

It can be seen that the frequency shift with the added mass is approximately linear and the errors in linearity can be owed to the positioning of the glass bead. From Eqs.1, the experimentally obtained effective modal mass $M_{eff,exp}$ for the third flexural mode is calculated and compared with the theoretical results as shown in Table I. It is observed that the experimentally and theoretically obtained M_{eff} are in close approximation.

The evaporation rate of a water droplet for contact angle below 40°is shown to stay constant by Hu et al.[28] with weak dependence on the contact angle. The evaporation rate for contact angle below 40°is given by Eqs.2. Hence, the frequency evolution from 352 s to 454 s is curve fitted to a linear polynomial and the evaporation rate of the water droplet $(\dot{m}_{exp})$ is calculated using Eqs.1 utilizing $M_{eff,exp}$. The video recording of the evaporating droplet is used to extract the contact angle

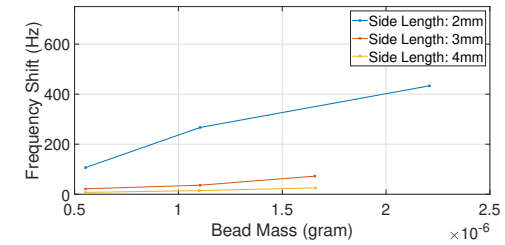

(a)

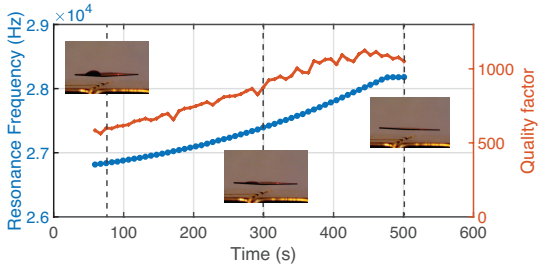

(b)

FIG. 2: **a)** The frequency shift of the third flexural mode of levitating plates of varying sizes associated with the placement of glass beads of known dimensions. **b)** The evolution of the third flexural resonance frequency and quality factor of a 4 mm levitating plate with the evaporation of 0.5 µL deposited on the anti-node with snapshots of the video recording.

Side Length	$M_{eff,th}$	$M_{eff,exp}$
4 mm	7.19×10^{-7} kg	9.15×10^{-7} kg
3 mm	3.64×10^{-7} kg	4.74×10^{-7} kg
2 mm	1.44×10^{-7} kg	1.73×10^{-7} kg

TABLE I: Effective modal mass obtained experimentally associated with the frequency shift of glass beads of diameter 75 µm; compared with the theoretical modal mass.

at 352 s and the evaporation rate is then obtained from Eqs.2, termed as $\dot{m}_{th}$.

$$-\dot{m}(t) = \pi r_b D(1-RH)c_v(0.27\theta^2+1.30) \tag{2}$$

where D is the vapor-phase diffusivity, r_b is the contact radius, c_v is the saturated vapor concentration on the droplet surface, RH is the relative humidity and θ is the contact angle. The temperature and RH are experimentally measured, and c_v and D are obtained from Rowan et al[29]. The numerical values of the parameters used for analysing droplet evaporation rate along with the obtained evaporation rates are shown in Table II. It can be seen that the evaporation rate obtained using frequency sweep analysis and using contact angle measured are in good approximation with error owing to positioning and inaccuracies in image processing measurement. The detailed analysis of water droplet evaporation rate can be found in SII.

The effect of droplet on the quality factor can be obtained

Temperature	21 °C	Contact Radius (r_b)	0.6164 mm
Relative Humidity	47 %	Diffusivity (D)	17 $mm^2\,s^{-1}$
Vapor Concentration (c_v)	1.9×10^{-8} $g\,mm^{-3}$	Contact Angle (th)	0.603 rad
$\dot{m}_f$	3.2×10^{-10} $kg\,s^{-1}$	$\dot{m}_f$	4.99×10^{-10} $kg\,s^{-1}$

TABLE II: Evaporation parameters

from the Eqs. 3.

$$\frac{1}{Q_{total}} = \frac{1}{Q_{vis}} + \frac{1}{Q_{plate}} \tag{3}$$

where Q_{total} is the total quality factor due to combined effect of viscous damping due to the added droplet (Q_{vis}) and the damping of the plate in air (Q_{plate}). Q_{plate} is taken as the quality factor at 500 s, while Q_{total} is taken as the quality factor at 59 s. Q_{vis} is then obtained to be 1245 using Eqs. 3. In comparison with the experimentally obtained damping due to added droplet, the theoretically obtained Q factor is 1513 from Eqs 4[30].

$$Q_{vis} = \rho_s H\sqrt{\frac{2\omega}{\eta\rho_f}}\frac{L^2}{A} \tag{4}$$

Where ρ_s is the density of the plate; H and L are the height and the length of the plate; ω is the resonance frequency of the plate at 59 s; η and ρ_l are the viscosity and density of the liquid taken as 1.002 mPa s and 997 $kg\,m^{-3}$ respectively. A is the contact area of the droplet experimentally obtained using image processing to be 1.39×10^{-4} m^2.

The precision of the mass sensor depends on the frequency stability of the oscillator. First to get the resonator into sustained oscillation, a phase lock loop leveraging Zurich instruments lock in amplifier as shown in Figure 1a is developed. The output signal from LDV is mixed with the signal generated by the numerically controlled oscillator (NCO) and demodulated after passing it through a low pass filter to obtain the phase. The phase is then fed to the PID controller for setpoint phase tracking. The output from the PID controller drives the NCO which in turn completes the loop by exciting the electromagnetic coil; which actuates the levitating plate into sustained oscillation.

The frequency stability of this diamagnetically levitated oscillator is analysed by measuring the Allan deviation ($\sigma_a(\tau)$) as a function of gate time τ (Eqs. 5), where $\langle ...\rangle$ is the expectation operator[31].

$$\sigma_a(\tau) = \frac{1}{f_0}\sqrt{\frac{1}{2}\langle(f_{n+1}-f_n)^2\rangle} \tag{5}$$

The plates of side length 2 mm, 3 mm and 4 mm levitating on an array of four cube magnets in diagonal orientation are developed as oscillators leveraging the phase lock loop defined above. The frequency output from the NCO is recorded for 60 s for three different points for different PID bandwidths for the third flexural mode. This frequency versus

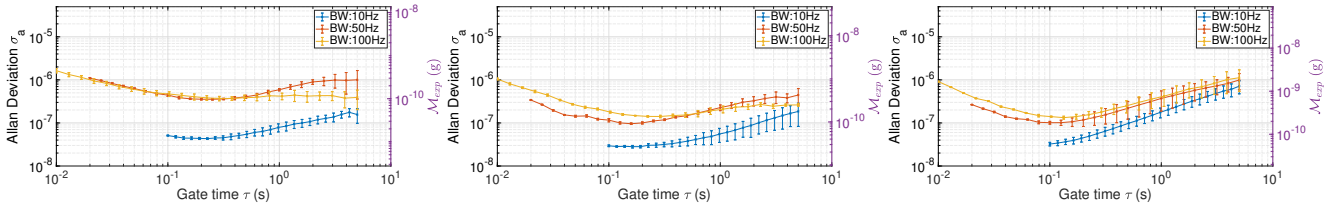

(a) (b) (c)

FIG. 3: **a)-c)** show the Allan deviation obtained for varying bandwidths for the square plates of side length 2 mm, 3 mm and 4 mm respectively along with the precision of mass sensing calculated by leveraging the effective modal mass obtained from Rayleigh Ritz method; using Eqs. 6 on the right axis. The Allan deviation is calculated from the frequency output generated by the NCO in the opto-electronic phase lock loop described in Figure 1a.

time signal is then split into packets of gate time τ. The average of each packet of signal is computed and termed as f_n for the nth packet. The Allan deviation of the frequency for the gate time τ is then computed using these f_n's given by Eqs. 5; where $\langle ... \rangle$ is the expectation operator. The Allan deviation for the three plates for varying bandwidths and gate times is shown in Figure 3.

It is seen that there is a presence of drift in the Allan deviation measurement. The cause of the drift at this moment is still unknown. It has been observed in previous work completed by Kumar et al[32], who attributed it to the LDV. The source of drift can also be dependent on many other factors such as thermal variations, continuous evaporation and condensation of water vapor, amplifier noise among many others. Further research needs to be conducted for a better understanding of the causes of these drifts. The Allan deviation was also measured for the second and third mode of the plate of side length 2mm and PID bandwidth of 10Hz and it was observed that the third mode as shown in Figure 1a is the most stable and has the best precision for the 4x4 diagonal levitation configuration shown in Figure 21a.

Finally, the experimental precision ($\mathscr{M}_{exp}$) of the mass sensor, dependent on Allan deviation is then computed using Eqs. (1). The experimentally obtained modal mass is utilized for the precision calculation, along with the minimum Allan deviation obtained from the frequency stability analysis.

$$\mathscr{M}_{exp} = 2M_{eff,exp}.\sigma_a(\tau) \tag{6}$$

where $\sigma_a(\tau)$ is the Allan deviation at gate time τ and $M_{eff,exp}$ is computed from the experimental analysis described above and shown in Table I.

The measured minimum Allan deviation and the corresponding precision $\mathscr{M}_{exp}$ of the third flexural mode for square levitating plates of side length 2 mm, 3 mm, 4 mm and thickness 100 µm, 90 µm, 80 µm respectively are shown in Figure 3. The minimum value of Allan deviation is utilized to compute the precision of the mass sensor; which is shown in Table III along with the corresponding gate time.

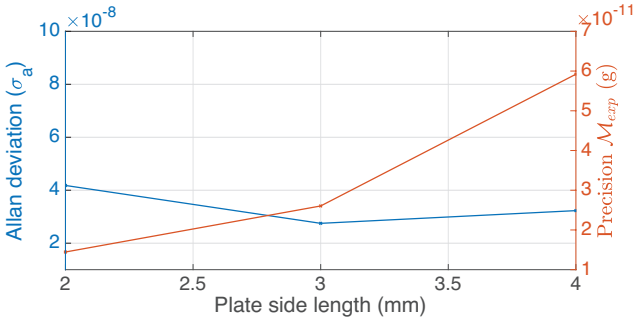

FIG. 4: The experimental precision of the levitating oscillators shown in red; obtained by Eqs.6 using the minimum Allan deviation for plates of different side length shown in blue.

Side Length (mm)	$\mathscr{M}_{exp}$ (pg)	Gate time (s)
2	14.4	0.10
3	26.0	0.17
4	59.2	0.18

TABLE III: Experimental Precision of mass sensor obtained from Eqs.6

In conclusion, we have shown that i) diamagnetically levitating plate can be modelled as a completely free free plate for the modelling of its flexural dynamics, ii) multi-modal analysis of the resonance frequencies and mode shapes of the levitated resonator can be used to extract the material properties of the plate; which shows that pyrolytic graphite is a naturally occurring auxetic material, iii) resonator based on diamagnetic levitation can be utilized as a mass sensor which has a precision of 14.4 pg for a gate time of 0.1 s for an instantaneous change in frequency iv) decrease in size leads to improved precision and iv) drift is present in the diamagnetically levitated oscillator with LDV based readout.

SUPPLEMENTARY INFORMATION

I. DYNAMICAL MODELLING OF LEVITATED PLATE

The levitating setup of our experiments mainly consists of a square plate of pyrolytic graphite levitating over a checkerboard arrangement of magnets with alternating magnetization as shown in Figure 5b. To obtain the required samples, a block of pyrolytic graphite is cleaved using scalpel to obtain thinner samples, which are then polished using sandpaper to obtain the required thickness. The thin polished sample is then cut into required in plane dimension using a laser cutter.

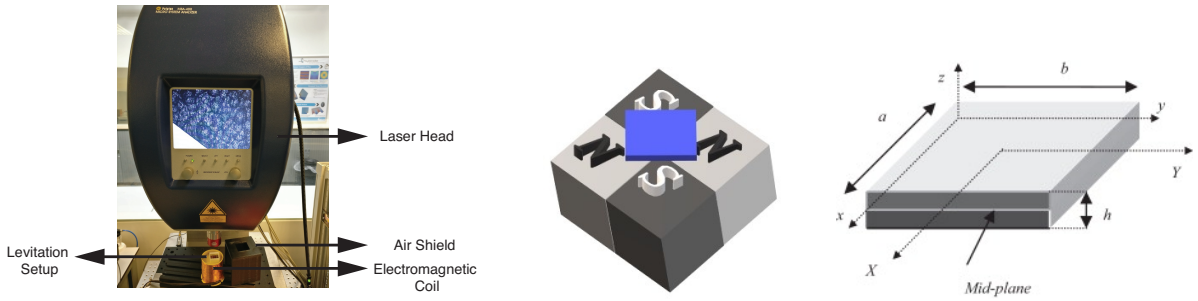

(a) (b) (c)

FIG. 5: **a)** The experimental setup showing the laser scanning head of the laser Doppler vibrometer along with the electromagnetic coil and levitation setup. A 3D printed shield is used to prevent movement due to flow of air. **b)** Checkerboard arrangement of cube magnets in alternating magnetization for stable diamagnetic levitation of a square pyrolytic graphite plate. **c)** The co-ordinate system for the dynamical modelling of a free free plate with a and b as in the in plane dimensions and h as the height of the plate.

An electromagnetic coil is used to actuate the levitating plate. The resonance frequencies and mode shapes are recorded using a laser Doppler vibrometer (LDV). In the first step of analysis, the effect of different magnetic configurations on the resonance frequencies of a levitating plate are analysed . Five different magnetic configurations as shown in Figure 6a are utilized to levitate a square plate of side length 12 mm and thickness 0.5 mm. The first three flexural resonance frequencies of the plate are recorded as seen in Figure 6b. It can be seen that the effect of different magnetic configurations on the resonance frequencies is negligible and therefore, the dynamical behaviour of the levitating plate can be modelled as a plate with free free boundary conditions[23].

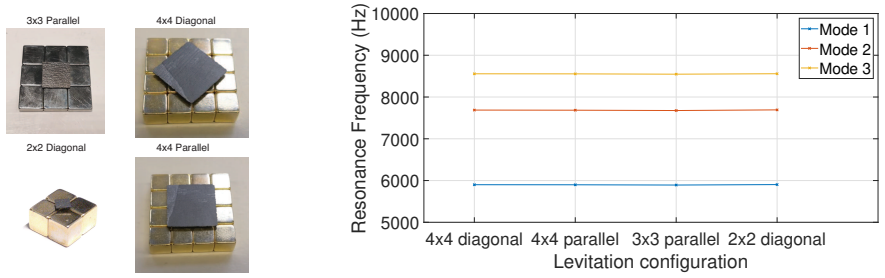

(a) (b)

FIG. 6: **a)** The different magnetic configuration used for levitation setup. The cubic array of 2 magnets are of side length 12 mm and residual magnetism of 1.42 T. The array of 3 cuboid magnets have the dimensions 10 mmx10 mmx1 mm residual magnetism of 1.32 T. The cubic array of 4 magnets are of side length 5 mm and residual magnetism of 1.32 T. **b)** The resonance frequencies of the first three flexural modes of a square pyrolytic graphite plate of side length 12 mm and thickness 0.42 mm for different magnetic configurations.

The dynamics of the plate have been modelled using two approaches: 1. Rayleigh Ritz method 2. Finite Element method. In the Rayleigh Ritz method; the plate is modelled with Kirchhoff Plate theory converting the problem into a two dimensional form with bending of the mid plane representative of the dynamical behaviour of the three dimensional plate. An orthogonal co-ordinate system with the origin at the corner of the mid plane of the plate is defined as shown in Fig 5c. The displacement at any point on the plate is expressed as[33]:

$$u(x,y,z,t) = u_0(x,y,t) - z\frac{\partial w_0}{\partial x} \tag{7}$$

$$v(x,y,z,t) = v_0(x,y,t) - z\frac{\partial w_0}{\partial y} \tag{8}$$

$$w(x,y,z,t) = w_0(x,y,t) \tag{9}$$

Considering small strains and moderate rotations, isotropic strain displacement relationships are denoted as :

$$\varepsilon_{xx} = \frac{\partial u_0}{\partial x} - z\frac{\partial^2 w_0}{\partial x^2} \tag{10}$$

$$\varepsilon_{yy} = \frac{\partial v_0}{\partial y} - z\frac{\partial^2 w_0}{\partial y^2} \tag{11}$$

$$\varepsilon_{xy} = \frac{\partial u_0}{\partial y} + \frac{\partial v_0}{\partial x} - 2\frac{\partial w_0}{\partial x \partial y} \tag{12}$$

And stress-strain relationships are evaluated in Eqs 13 with E as the Young's modulus and ν_{xy} as the in plane Poisson's ratio.

$$\begin{Bmatrix} \sigma_x \\ \sigma_y \\ \tau_{xy} \end{Bmatrix} = \begin{pmatrix} \frac{E}{1-\nu_{xy}^2} & \frac{\nu_{xy}E}{1-\nu_{xy}^2} & 0 \\ \frac{\nu_{xy}E}{1-\nu_{xy}^2} & \frac{E}{1-\nu_{xy}^2} & 0 \\ 0 & 0 & \frac{E}{2(1+\nu_{xy})} \end{pmatrix} \begin{Bmatrix} \varepsilon_{xx} \\ \varepsilon_{yy} \\ \gamma_{xy} \end{Bmatrix} \tag{13}$$

The kinetic energy of the plate is then calculated as:

$$T_p = \frac{1}{2}\rho h \int_0^a \int_0^b (\dot{u_0}^2 + \dot{v_0}^2 + \dot{w_0}^2) dxdy \tag{14}$$

where overdot represent time derivative, T_p is the kinetic energy of the system; a and b are the in-plane dimensions of the plate and h is the thickness of the plate. The elastic potential energy of the plate is given as:

$$U_p = \frac{1}{2}\int_{-\frac{h}{2}}^{\frac{h}{2}} \int_0^a \int_0^b (\sigma_x\varepsilon_x + \sigma_y\varepsilon_y + \tau_{xy}\gamma_{xy}) dxdydz \tag{15}$$

With the assumption of synchronous vibration, the displacement field of the plate can be expressed as[34,35]:

$$u_0(x,y,t) = U(x,y)g(t) \tag{16}$$

$$v_0(x,y,t) = V(x,y)g(t) \tag{17}$$

$$w_0(x,y,t) = W(x,y)g(t) \tag{18}$$

Here, the functions $U(x,y), V(x,y), W(x,y)$ denotes the mode shapes while $g(t)$ is the harmonic time function, which remains constant for all displacements. The mode shapes are approximated using ordinary polynomial functions[36]:

$$U(\eta,\zeta) = \sum_{m=0}^{M}\sum_{n=0}^{N} A_{mn}\eta^m\zeta^n \tag{19}$$

$$V(\eta,\zeta) = \sum_{q=0}^{Q}\sum_{r=0}^{R} B_{qr}\eta^m\zeta^n \tag{20}$$

$$W(\eta,\zeta) = \sum_{k=0}^{S}\sum_{l=0}^{T} C_{st}\eta^m\zeta^n \tag{21}$$

where $\eta = x/a$ and $\zeta = y/b$ represent dimensionless variables. The unknown coefficients are compiled to form a vector $\boldsymbol{q}$ to solve the linear equation of motion:

$$q = [A_{00},...,A_{MN},B_{00},...,A_{QR},C_{00},...,C_{ST}] \tag{22}$$

The size of the vector $\boldsymbol{q}$ is termed the number of degrees of freedom and is denoted as N_{dof}:

$$N_{dof} = (M+1)(N+1) + (Q+1)(R+1) + (S+1)(T+1) \tag{23}$$

The Lagrangian functional $L = T_p - U_p$ is minimized in the Rayleigh Ritz method by utilizing the Lagrange equations of motion (Eqs. 24); with the assumption that $\boldsymbol{g}(t) = \boldsymbol{q}g(t)$ with $g(t) = \exp(j\omega t)$, where ω is the natural frequency of vibration and j is the unit imaginary number.

$$\frac{d}{dt}\frac{\partial L}{\partial \dot{\boldsymbol{g}}_k} - \frac{\partial L}{\partial \boldsymbol{g}_k} = 0, \qquad k = 1,...,N_{dof} \tag{24}$$

Since, levitating graphite plate can be assumed to be a completely free plate, only the geometric boundary conditions are required to be fulfilled. Thereby, no constraints have been put on the polynomials. Assembling the equations of motions for the unknown variables leads to the formulation of the dynamical equation of motion (Eqs. 25).

$$(-\omega^2 \boldsymbol{M} + \boldsymbol{K})\boldsymbol{q} = 0 \tag{25}$$

Where, ω is the natural frequency of vibration, M is the mass matrix and K is the stiffness matrix. The Rayleigh Ritz approach of dynamical modelling of levitated plate is implemented in Mathematica 11.3 software to build the equations of motion and obtain the vibration frequencies and mode shapes of the plate.

The equation of motion is solved using an eigenvalue analysis and the resonance frequencies (ω) and eigenvectors (ϕ) are computed. The effective modal mass (M_{eff}) of different mode shapes are then computed. The mode shape $W^i(x,y)$ associated with i^{th} mode is reconstructed by substituting the unknown coefficients C with the calculated eigenvector (ϕ^i).The mode shape is then normalized with $max[W^i(x,y)] = 1$. The equation of motion for a single degree of freedom with the normalized mode shape is then computed using the Lagrangian equation of motion as described above. The obtained mass matrix is then the effective modal mass of the selected flexural mode ($M_{eff,th}$).

The dynamical behaviour of levitated plate is also modelled leveraging finite element method in COMSOL Multiphysics with solid mechanics study and quadratic serendipity discretization. A mapped mesh with 30 elements in the thickness dimension with free tetrahedral elements is used to conduct a reduced order modal analysis to build the system matrices and obtain the mode shapes and vibration frequencies of the plate.

The eigenvectors are scaled to maximum value to obtain the reduced order model for the first nine resonance frequencies; which includes first six rigid body modes and first three flexural modes. The obtained mass matrix then provides the M_{eff} for different modes. It is observed that the M_{eff} obtained from the Rayleigh Ritz approach and Finite Element method are the same and are termed as $M_{eff,th}$ shown in Table I.

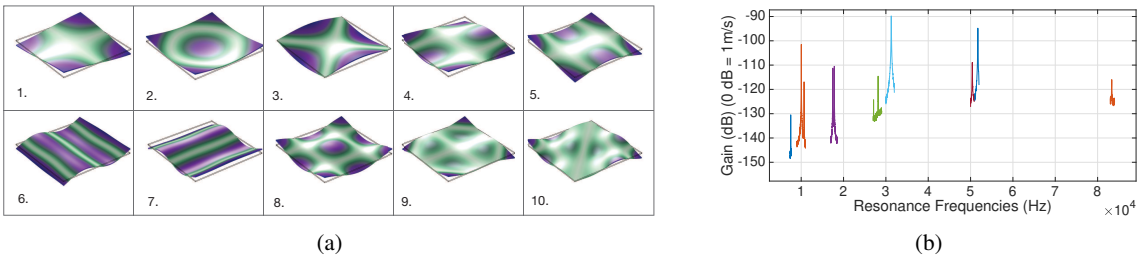

(a) (b)

FIG. 7: **a)** Simulations of the first ten mode shapes of a levitating pyrolytic graphite plate with dimensions 6 mmx6 mmx0.1 mm obtained with electromagnetic actuation and observed using laser Doppler vibrometer. **b)** The frequency response curve of the first ten flexural modes of a square levitating plate of side length 6 mm levitating on 4x4 parallel magnetic configuration in correspondence with the mode shapes are shown.

The first eleven modes shapes and natural frequencies of vibration of a levitating square plate of side length 6 mm and thickness 100 µm are recorded leveraging LDV and the first ten modes are shown in Figure 7. The material properties of the levitating graphite plate are obtained by minimizing the root mean square error (e_{rms}) of theoretically and experimentally obtained vibration frequencies (Eqs.26). The Young's modulus (E) and the Poisson's ratio (ν_{xy}) are taken as design variables for the optimization problem, with the Rayleigh Ritz and Finite Element Method utilized to obtain the theoretical natural frequencies of vibration. Sequential quadratic programming algorithm is utilized to find the minima of the optimization problem leveraging MATLAB R2018a. The optimization is conducted in two steps. First, the rms error in frequency ratios normalized to the first flexural mode is minimized to obtain ν_{xy}. The obtained ν_{xy} is fed into the model to minimize the rms error of the resonance frequencies with the Young's modulus as the design variable.

$$e_{rms} = \sqrt{\frac{1}{N}\sum_{i=0}^{N}(\omega_{exp,i} - \omega_{th,i})^2} \tag{26}$$

where ω_{th} and ω_{exp} are the theoretically and experimentally obtained natural frequencies of vibration.

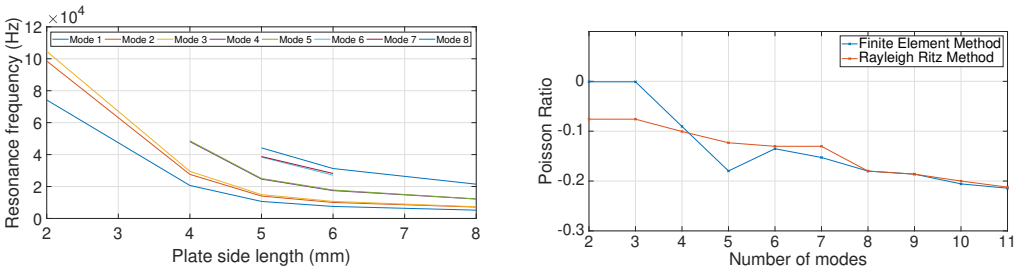

(a) (b)

FIG. 8: **a)** The variation of resonance frequencies of levitating square plate with varying side length is plotted for the first seven flexural modes. **b)** The Poisson's ratio of the pyrolytic graphite plate obtained using an optimization algorithm by minimizing the root mean square error between the experimental and theoretically (Rayleigh Ritz method and FEM Simulation) obtained normalized frequency ratios with increasing number of mode shapes taken into consideration.

The optimization problem is solved by including increasing number of mode shapes for better convergence as seen in Figure 8b. The Young's modulus and in plane Poisson's ratio then obtained from Finite Element Method and Rayleigh Ritz method are in close match; and converge to $E = 39.3\,\text{GPa}$ and $\nu_{xy} = -0.2122$. The results obtained are concurrent with the values reported in literature, wherein pyrolytic graphite is termed as a naturally occurring auxetic material[37].

The in-plane negative Poisson's ratio can be explained by the production and structure of pyrolytic graphite. Pyrolytic graphite is a poly crystalline form of graphite which is produced by deposition of simple hydrocarbons like methane at high temperatures. This process forms wrinkled and wave like layers of hexagonal structured hydrocarbon. The wrinkles can then be attributed to the negative in plane Poisson's ratio as similarly seen in graphene membranes[26,27]. Such an effect, therefore leads to positive Poisson's ratio out of plane as reported by Bert et al.[37]. Isostatic graphite, on the other hand is a fine grain graphite produced by isostatic pressing of coke filler in a binder material high pressure. Thereby, imparting it averaged properties in all directions, leading to a positive Poisson's ratio[38].

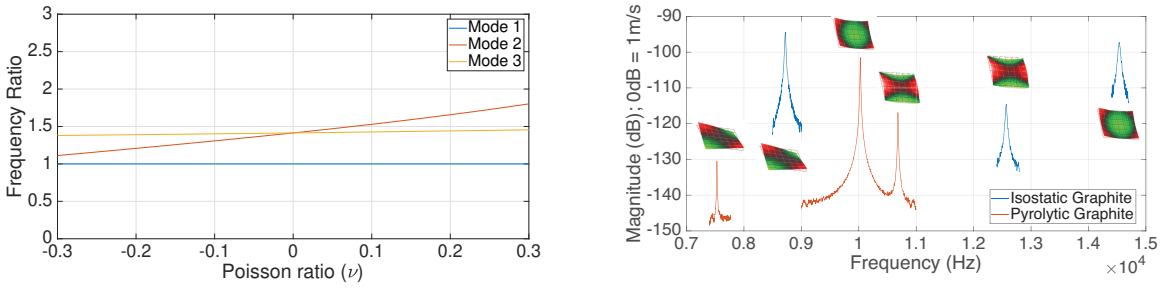

(a) (b)

FIG. 9: **a)** The frequency ratios of the second and third mode in comparison with the first mode with varying Poisson's ratio predicted by the Rayleigh Ritz model. **b)** The sequence of modes observed for levitating pyrolytic graphite plate and isostatic graphite plate and the observed mode crossing.

The auxetic in plane behaviour is then verified by observing the sequence of the first three mode shapes in levitating isostatic graphite plate and the pyrolytic graphite plate. The mode crossing of the second and the third mode occurs at $\nu_{xy} = 0$ obtained using the Rayleigh Ritz method as shown in Figure 9a. The sequence of the modes of the first three resonance frequencies of a levitating plate of isostatic graphite and pyrolytic graphite was observed. The isostatic graphite plate has a Poisson ratio of 0.23

as obtained from the supplier data. Upon actuation and readout of flexural modes of the isostatic graphite plate, it was observed that the second mode and the third mode were in reverse order (Figure 9b) compared to the pyrolytic graphite plate, as predicted by the theoretical model.

The convergence analysis of the Mathematica model and COMSOL model is performed for the first three modes with respect to degree of freedom and maximum mesh element size respectively as shown in Figure 10. In the Mathematica model, the percentage error for the first three flexural modes obtained with N_{dof} varying from 27 to 147 with respect to the flexural modes at 192 N_{dof} is presented. In the finite element model mesh refinement study, the error percentage of the first three flexural modes with varying mesh element size with respect to the flexural modes at a maximum mesh element size of 0.03*mm* are evaluated. It can be concluded that the Rayleigh Ritz and FEM implementation with 147 N_{dof} and maximum element size of 0.05*mm* respectively are converged and valid for the optimization problem

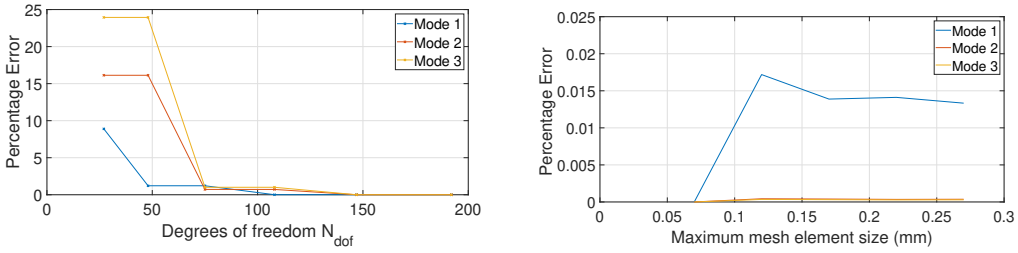

(a) (b)

FIG. 10: The convergence of first three flexural resonance frequencies of a square plate of side length 2 mm with increasing number of degrees of freedom in Rayleigh Ritz method and decreasing maximum mesh element size in the Finite element model.

The rigid body motion of the magnets upon electromagnetic excitation was also recorded and gives a deeper understanding about the actuation mechanism of the levitating pate. The rigid body motion of 2x2 and 4x4 array of magnets was recorded using LDV and the obtained frequency response in shown in Figure 11.

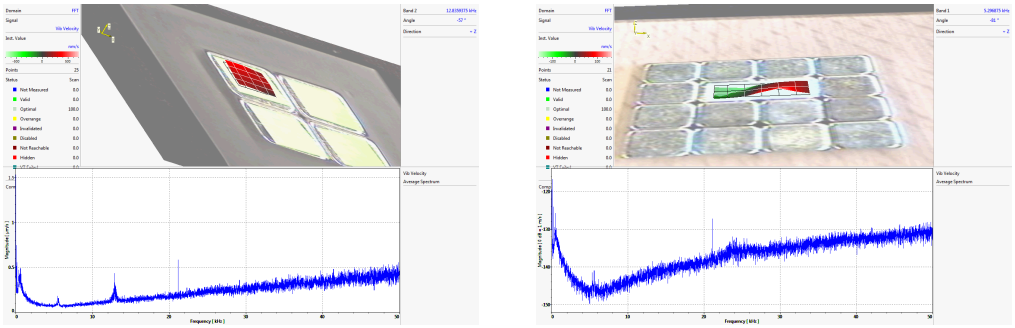

(a) (b)

FIG. 11: a) The recorded rigid body motion of one magnet in 2x2 array of cube magnets of side length 12*mm* actuated using electromagnetic coil and read out using LDV. **b)** The observed rigid body motion of 2 magnets in a 4x4 array of cube magnets in alternating magnetization and of side length 12*mm* actuated using electromagnetic coil and read out using LDV.

Apart from observing resonance frequencies of levitating plate in air, the resonance frequencies and mode shapes of diamagnetically levitated plate levitating in water was also observed as shown in Figure 12a. A square plate of side length 12*mm* and thickness 0.42*mm* levitating on top of 2x2 magnet array in diagonal orientation submerged in water; and is excited in its third resonance mode as shown in Figure 12a. The levitation of the plate submerged in water in an aluminium container with the magnets situated outside the beaker has also been shown in Figure 12b; showcasing the possibility of separation of the electronic component and the sensing element even in liquid medium. Hence, the possibility of developing oscillator based sensors in liquid is a potential future application for a diamagnetically levitated resonator.

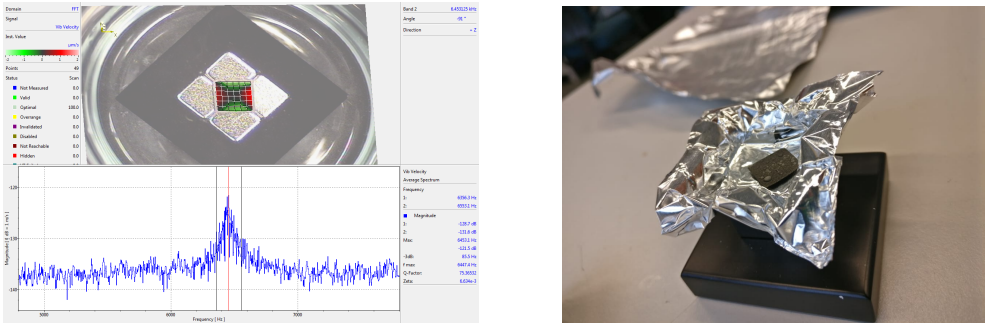

(a) (b)

FIG. 12: **a)** The third flexural mode of a square pate of side length 12*mm* and thickness 0.42*mm* levitating on 2x2 diagonal configuration, submerged in water. **b)** In this case, only the levitating plate is submerged in water in an aluminium beaker.

II. OSCILLATOR SENSITIVITY ANALYSIS

The postcolumn reactor components, acid washed glass beads of diameter 75 µm were obtained from sigma Aldrich for mass sensitivity calibration. The frequency shift of the third flexural mode on the placement of the glass beads was measured using the sweep function of the Zurich Instruments lock in amplifier. The frequency sweep was conducted before placing the glass bead, after placing the glass bead and after removal of the glass bead. The average difference of the frequency shift between the frequency with the glass bead compared to the resonance frequencies measured without the glass bead was utilized to compute the effective modal mass as shown in Table I. The diameter of the glass bead is assumed to be constant as 75 µm for the effective modal mass calculation. The resonance frequencies of the third flexural mode associated with and without the glass bead are plotted in Figures 13-15.

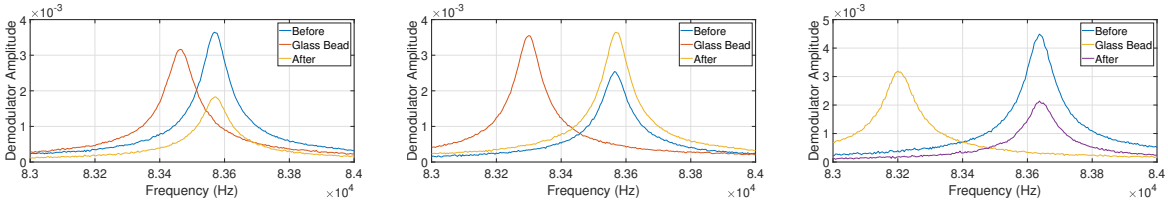

(a) (b) (c)

FIG. 13: **a)-c)** shows the frequency shift of the third flexural mode associated with placing 1,2 and 4 bead(s) respectively on the plate of side length 2mm.

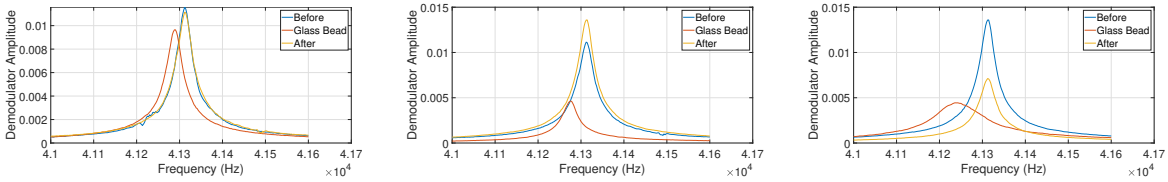

(a) (b) (c)

FIG. 14: **a)-c)** shows the frequency shift of the third flexural mode associated with placing 1,2 and 3 bead(s) respectively on the plate of side length 3mm.

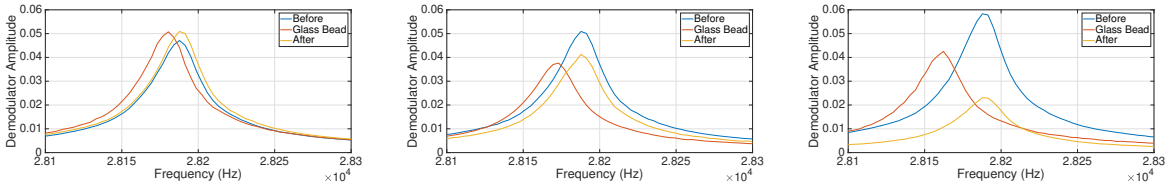

(a) (b) (c)

FIG. 15: **a)-c)** shows the frequency shift of the third flexural mode associated with placing 1,2 and 3 bead(s) respectively on the plate of side length 4mm.

The evaporation rate of droplet of volume 0.55 µl was measured by analysing the frequency versus time evolution for the third flexural mode and by using video recording in combination with the finite element model develop by Hu et al.[28]. The video recorded from the digital microscope is first calibrated for pixel to meter conversion using the magnet as the calibration object. It is found that 1 pixel corresponds to 7.46×10^{-6} m. For evaluating the droplet contact angle (θ), the video frame at 352s is extracted and the height (h) and contact radius (r_b) of the droplet is calculated by counting the number of pixels for the same. The contact angle of the droplet is then calculated using Eqs. 27[39].

$$h = r_b tan(\frac{\theta}{2}) \tag{27}$$

The geometric representation of the spherical droplet geometry is shown in Figure 16, along with the image processing measurements for t=60s and 350s.

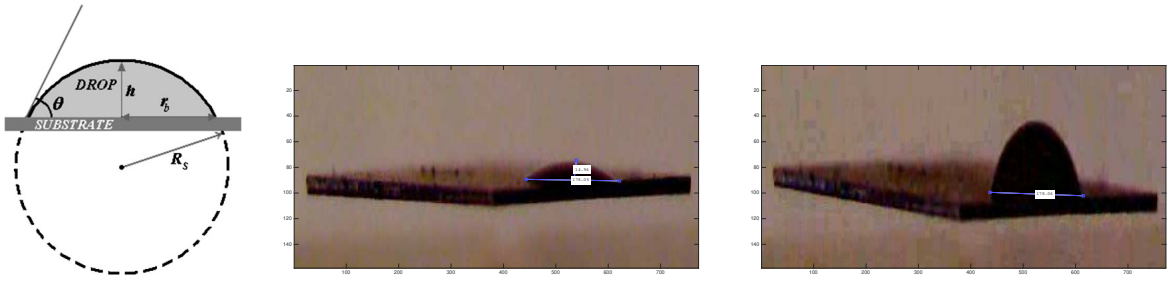

(a) (b) (c)

FIG. 16: **a)**The geometrical representation of the spherical droplet assumption for the purposes of calculation the contact angle and contact area[39]. **b)** The image processing results of the calculation of the contact radius and height of the evaporating droplet presented in Table II at time 353s. **b)** The image processing results for the calculation of the contact area for the calculation of the viscous damping effect due to the added droplet.

The Q factor of the resonance frequency was estimated by fitting the response of a single degree of freedom mass spring damper to the recorded resonance frequency response function. The frequency evolution of the third flexural modes of the plate of side length 4 mm was also conducted with varying droplet volumes as shown in Figure 17a. It could be seen that the evaporation time of droplets of varies linearly with the varying volumes.

The effect of position of the placed droplet on the evolution of the frequency of the third flexural mode for a square levitating plate of side length 4 mm and thickness 105 µm was also observed as shown in Figure 17b. It is important to note that a different 4mm sample was utilized for this study to preserve the original 4mm sample for further study. The droplet was deposited on two different locations, namely near the center of the plate (node) and near the centre of the edge (anti-node). And the difference in the frequency shift can be clearly observed due to this position dependency. The placement of the droplet is a completely manual process. The plate was plasma cleaned for the third trial before putting the droplet near the anti-node of the third flexural mode. After plasma cleaning, the surface of the plate becomes extremely hydrophilic causing the droplet to obtain a very small contact angle.

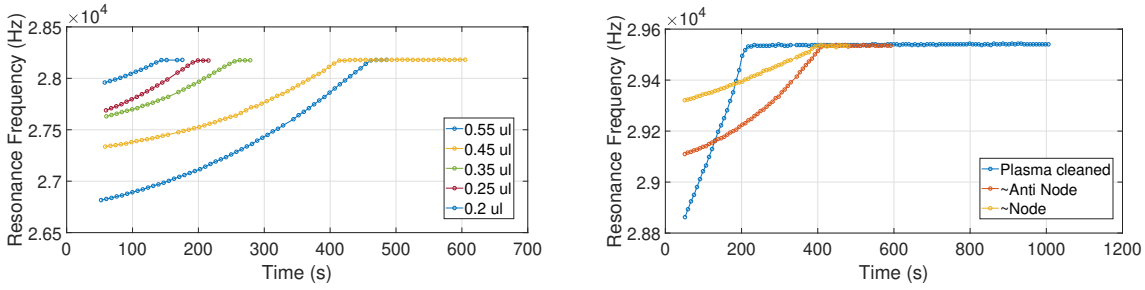

(a) (b)

FIG. 17: **a)** The evolution of the third resonance frequency of the plate of side length 4mm with varying volumes dispensed using a precision Eppendorf pipette. **b)** The effect of position on the frequency evolution of the third flexural resonance frequency for the second sample plate of side length 4mm. The plate was plasma cleaned to increase the hydrophilicity. A 0.55 µl droplet was then dispensed on the plasma cleaned plate, causing the droplet to attain a relatively low contact angle and hence a linear evaporation rate.

The linear fit for the evaporation rate of the 0.55 µl droplet as shown in Figure 2 and presented in Table II is shown in Figure 18a. The evaporation rate for the low contact angle droplet obtained after plasma cleaning is completely linear as predicted by Hu et al.[28]. The evaporation rate for this low contact angle droplet evaporation is found to be $2.443 \times 10^{-10}\,\mathrm{kg\,s^{-1}}$ utilizing Eqs. 1. The effective modal mass is assumed to be the same as given in Table I. The difference in evaporation rate can be attributed to a bigger spread of the droplet, leading to position dependent inaccuracies. The linear fit for the calculation of the evaporation

rate is shown in Figure 18b.

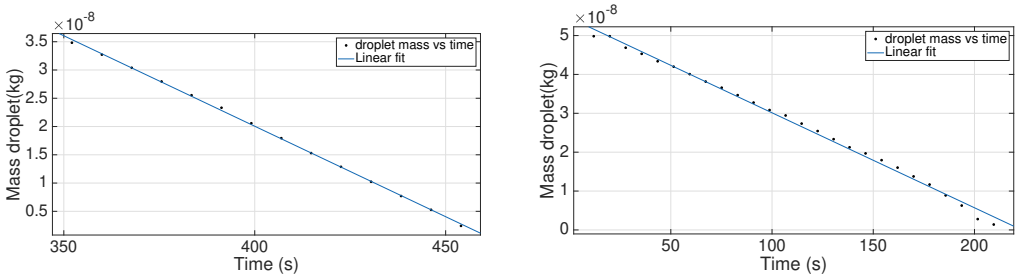

FIG. 18: **a)** The linear fit for mass versus time as obtained from the frequency evolution of the third flexural mode for a droplet of initial volume 0.55 µl. The experimentally obtained effective modal mass in conjunction Eqs. 1 is utilized to get the mass versus time plot. **b)** The linear fit for mass versus time as obtained from the frequency evolution of the third flexural mode for a droplet of initial volume 0.55 µl deposited on a plasma cleaned square levitating plate of side length 4mm. The experimentally obtained effective modal mass in conjunction Eqs. 1 is utilized to get the mass versus time plot.

This section will elaborate more on the frequency stability and mass precision analysis conducted for evaluation of mass sensitivity of a diamagnetically levitated oscillator. The picture of the actual experimental setup is shown in Figure 19a. The levitating pyrolytic graphite plate is actuated using an electromagnetic coil. A 3D printed air shield is utilized to prevent vibrations due to air flow. The LDV reads out the frequency response and feeds it to the Zurich Instrument lock-in-amplifier denoted by the signal input in Figure 19b. The signal input is then mixed with the signal generated from the numerically controlled oscillator and passed through a low pass filter to obtain the phase and magnitude of the signal input. The phase is then fed into a PID controller, which tracks the set-point phase of the resonance. The signal generated from the PID controller drives the numerically controlled oscillator which then feeds it to the electromagnetic coil for the actuation of the levitating plate. Hence, an oscillator is developed employing a phase lock loop.

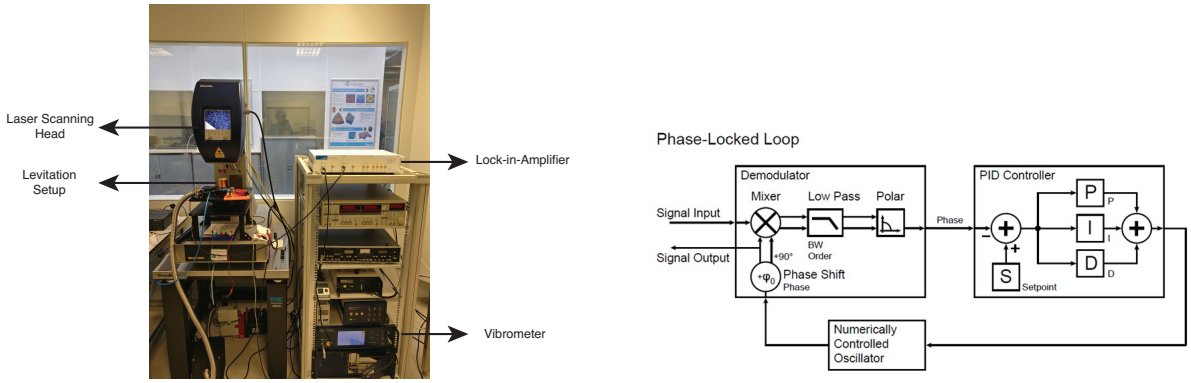

FIG. 19: **a)** The picture of the actual experimental setup as described in Figure 1a. **b)** The detailed schematic of the phase lock loop along with the PID control loop utilized to develop the oscillator.

The standard deviation is not a good measure to analyse the frequency stability of oscillators because it is dependent on recorded sample size (N) and does not converge for certain types of noises, which are prevalent in oscillators. Therefore, Allan deviation is the preferred statistical measure compared to the standard deviation for analysing the frequency stability of oscillators. First to compute the Allan deviation, the normalized frequency (y[n]) is computed as :

$$y[n] = \frac{f[n] - f_0}{f_0} \tag{28}$$

Where, f_0 is the mean resonance frequency of the recorded frequency signal, $f[n]$ is the frequency output of the NCO in the phase lock loop at n^{th} data point. The Allan deviation is a function of gate time. The Allan deviation is calculated from the slowest of the timescales among the PID Controller, Sampling rate and Low Pass Filter (minimum frequency). The normalized frequency versus time signal is split into sections of data points corresponding to the selected gate time τ. The gate time is always an integer multiple of the sampling time (T_s) i.e.; $\tau = cT_s$. The average of these sections is then calculated and termed as $\overline{y[m]}$. The normalized frequency versus time signal with sampling frequency 1717 Hz, along with the averaged normalized frequency for a gate time of 0.1048 s is shown in Figure 20a. The Allan deviation is then calculated as:

$$\sigma_a = \sqrt{\frac{1}{2(M-1)} \sum_{m=1}^{M} (\overline{y[m+1]} - \overline{y[m]})^2} \tag{29}$$

Where, $M = N/c$, since the recorded sample size N is divided into sections of c data points.

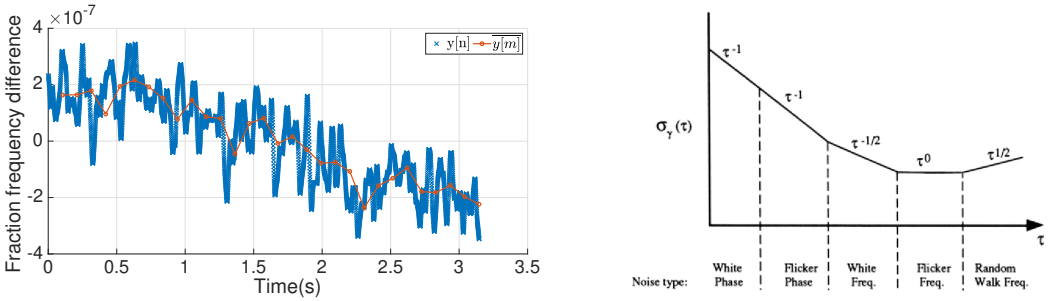

(a) (b)

FIG. 20: **a)** The blue trace showcases the normalized frequency (y[n]) versus time signal obtained from the frequency output of the phase lock loop of the levitating oscillator of side length 2mm. The red trace is the average values of the sectioned nominal frequency signal for a gate time of 0.104s. **b)** The slope of Allan deviation provides information about the type of noise predominant in the system[40].

The Allan deviation for the second and third flexural resonance of the plate of side length 2mm leveraging the phase lock loop described above is shown in Figure 21a. The minimum Allan deviation obtained for the second mode is 1.54×10^{-6}. The effective modal mass of the 2mm plate for the second flexural mode is 8.94×10^{-8} kg. From the experimentally obtained Allan deviation and theoretical effective modal mass obtained using Rayleigh Ritz method; the precision of the second flexural mode for mass sensing is calculated using Eqs. 6 to be 276 pg. The Allan deviation of the different plates with a PID control BW of 10Hz is plotted in Figure 21b.

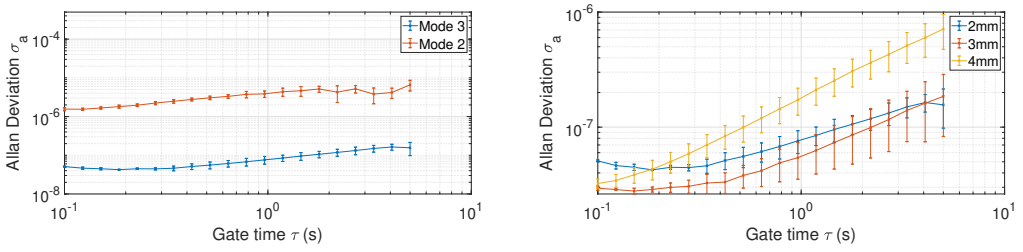

(a) (b)

FIG. 21: **a)** The Allan deviation of second and third flexural mode of a levitating oscillator of side length 2mm measured using the raw frequency output from the phase lock loop. **b)** The overlay of the Allan deviation of the levitating oscillators of side length 2mm, 3mm and 4mm measured utilizing the phase lock loop.

The noise in an oscillator is predominantly of five types: white phase noise, flicker phase noise, white frequency, flicker frequency and random walk frequency[40]. The slope of Allan deviation is utilized to identify the type of noise present in the oscillator. The measured Allan deviation with a PID control bandwidth of 100 Hz is shown for the three plate samples of side length 2*mm*,3*mm* and 4*mm* respectively in Figure 22. It can be seen in the small timescales ($\tau \leq 1$), the noise source is predominantly white frequency noise as the slope of the curve is proportional to $\tau^{-0.5}$. The drift observed in the longer

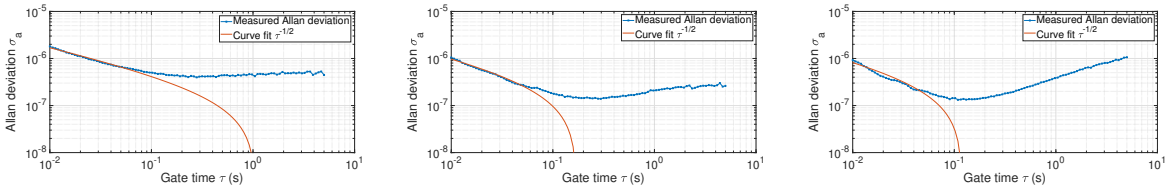

(a) (b) (c)

FIG. 22: **a)-c)** showcase the Allan deviation of levitating oscillators of side length 2mm,3mm and 4mm respectively with a PID control bandwidth of 100Hz. The slope of small timescales is proportional to $\tau^{-0.5}$ as obtained by curve fitting. It can be therefore commented that the noise at the small timescales is predominantly white frequency noise.

timescales ($\tau \geq 1$) cannot be commented upon this moment and requires further analysis.

The phase noise spectrum of the closed phase lock loop is computed using Zurich Instruments lock-in-amplifier as shown in Figure 23. The phase noise spectrum needs to be further analysed to understand the sources of drift in the system. The dynamics of the closed loop also influence the complete oscillator system; which needs to be analysed for a clearer understanding of the drift in the oscillator.

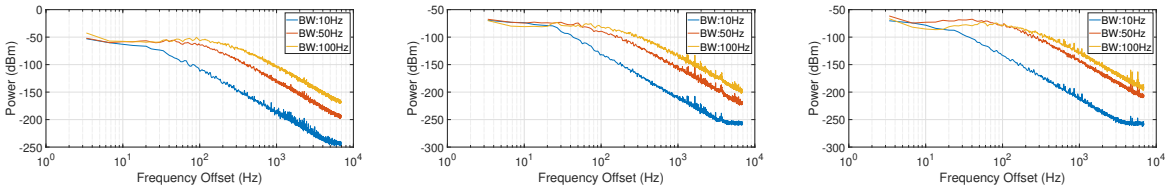

(a) (b) (c)

FIG. 23: **a)-c)** showcase the phase noise spectrum of the phase lock loop of the 2mm, 3mm and 4mm plate respectively.

[1]B. Ando, S. Baglio, and G. L'Episcopo, "A low-cost, disposable, and contactless resonant mass sensor," IEEE Transactions on Instrumentation and Measurement **62**, 246–252 (2013).
[2]R. Fogel and J. Limson, "Developing biosensors in developing countries: South Africa as a case study," (2016).
[3]S. Sharma, J. Zapatero-Rodríguez, P. Estrela, and R. O'Kennedy, "Point-of-Care diagnostics in low resource settings: Present status and future role of microfluidics," (2015).
[4]E. H. Brandt, "Levitation in physics." Science (New York, N.Y.) **243**, 349–55 (1989).
[5]L. M. Hauzer, "Mass and stiffness measurement using a multi-modal analysis," (2017).
[6]S. A. Zhgoon, A. S. Shvetsov, S. A. Sakharov, and O. Elmazria, "High-Temperature SAW Resonator Sensors: Electrode Design Specifics," IEEE Transactions on Ultrasonics, Ferroelectrics, and Frequency Control **65**, 657–664 (2018).
[7]M. V. Berry and A. K. Geim, "Of flying frogs and levitrons," European Journal of Physics **18**, 307–313 (1997).
[8]M. D. Simon and A. K. Geim, "Diamagnetic levitation: Flying frogs and floating magnets (invited)," Journal of Applied Physics **87**, 6200–6204 (2000).
[9]M. D. Simon, L. O. Heflinger, and A. K. Geim, "Diamagnetically stabilized magnet levitation," American Journal of Physics **69**, 702–713 (2001).
[10]S. Palagummi and F. G. Yuan, "An optimal design of a mono-stable vertical diamagnetic levitation based electromagnetic vibration energy harvester," Journal of Sound and Vibration **342**, 330–345 (2015).
[11]S. V. Palagummi and F. G. Yuan, "An enhanced performance of a horizontal diamagnetic levitation mechanism-based vibration energy harvester for low frequency applications," Journal of Intelligent Material Systems and Structures **28**, 578–594 (2017).
[12]S. Palagummi and F. G. Yuan, "A bi-stable horizontal diamagnetic levitation based low frequency vibration energy harvester," Sensors and Actuators, A: Physical **279**, 743–752 (2018).
[13]H. Chetouani, H. Rostaing, G. Reyne, C. Jeandey, V. Haguet, and C. Dieppedale, "Diamagnetic Levitation With Permanent Magnets for Contactless Guiding and Trapping of Microdroplets and Particles in Air and Liquids," IEEE Transactions on Magnetics **42**, 3557–3559 (2006).
[14]C. Pigot, H. Chetouani, G. Poulin, and G. Reyne, "Diamagnetic levitation of solids at microscale," in *IEEE Transactions on Magnetics*, Vol. 44 (2008) pp. 4521–4524.
[15]S. Clara, H. Antlinger, A. Abdallah, E. Reichel, W. Hilber, and B. Jakoby, "An advanced viscosity and density sensor based on diamagnetically stabilized levitation," Sensors and Actuators, A: Physical **248**, 46–53 (2016).
[16]R. Pelrine, A. Wong-Foy, B. McCoy, D. Holeman, R. Mahoney, G. Myers, J. Herson, and T. Low, "Diamagnetically levitated robots: An approach to massively parallel robotic systems with unusual motion properties," in *Proceedings - IEEE International Conference on Robotics and Automation* (IEEE, 2012) pp. 739–744.
[17]D. Garmire, H. Choo, R. Kant, S. Govindjee, C. H. Séquin, R. S. Muller, and J. Demmel, "Diamagnetically levitated MEMS accelerometers," in *TRANSDUCERS and EUROSENSORS '07 - 4th International Conference on Solid-State Sensors, Actuators and Microsystems* (IEEE, 2007) pp. 1203–1206.
[18]A. K. Geim and H. A. Ter Tisha, "Detection of earth rotation with a diamagnetically levitating gyroscope," Physica B: Condensed Matter **294-295**, 736–739 (2001).
[19]J. Abadie, E. Piat, S. Oster, and M. Boukallel, "Modeling and experimentation of a passive low frequency nanoforce sensor based on diamagnetic levitation," Sensors and Actuators, A: Physical **173**, 227–237 (2012).
[20]A. Keşkekler, *Characterization and Dynamics of Diamagnetically Levitated Objects*, Ph.D. thesis (2018).
[21]Y. Xu, Q. Cui, R. Kan, H. Bleuler, and J. Zhou, "Realization of a Diamagnetically Levitating Rotor Driven by Electrostatic Field," IEEE/ASME Transactions on Mechatronics **22**, 2387–2391 (2017).
[22]I. Simon, A. G. Emslie, P. F. Strong, and R. K. McConnell, "Sensitive tiltmeter utilizing a diamagnetic suspension," Review of Scientific Instruments **39**, 1666–1671 (1968).
[23]A. W. Leissa, *NASA SP* (1969) arXiv:arXiv:1011.1669v3.
[24]C. Bert, "Unusual poisson's ratios of pyrolytic graphite." AIAA Journal **7**, 1814–1815 (1969).
[25]J. M. BERRY and J. GEBHARDT, "Mechanical properties of pyrolytic graphite," AIAA Journal **3**, 302–308 (2008).
[26]V. H. Ho, D. T. Ho, S. Y. Kwon, and S. Y. Kim, "Negative Poisson's ratio in periodic porous graphene structures," Physica Status Solidi (B) Basic Research **253**, 1303–1309 (2016).
[27]J. N. Grima, S. Winczewski, L. Mizzi, M. C. Grech, R. Cauchi, R. Gatt, D. Attard, K. W. Wojciechowski, and J. Rybicki, "Tailoring graphene to achieve negative poisson's ratio properties," Advanced Materials **27**, 1455–1459 (2015).
[28]H. Hu and R. G. Larson, "Evaporation of a sessile droplet on a substrate," Journal of Physical Chemistry B **106**, 1334–1344 (2002).
[29]S. M. Rowan, M. I. Newton, and G. McHale, "Evaporation of microdroplets and the wetting of solid surfaces," Journal of Physical Chemistry **99**, 13268–13271 (1995).
[30]A. T. H. Lin, J. Yan, and A. A. Seshia, "Dynamic response of water droplet coated silicon MEMS resonators," in *Proceedings - IEEE Ultrasonics Symposium* (2009).
[31]J. A. Barnes, A. R. Chi, L. S. Cutler, D. J. Healey, D. B. Leeson, T. E. Mcgunigal, J. A. Mullen, W. L. Smith, R. L. Sydnor, R. F. C. Vessot, and G. M. R. Winkler, "Characterization of Frequency Stability," Tech. Rep.
[32]L. Kumar, K. Reimann, M. J. Goossens, W. F. Besling, R. J. Dolleman, R. H. Pijnenburg, C. Van Der Avoort, L. P. Sarro, and P. G. Steeneken, "MEMS oscillating squeeze-film pressure sensor with opto-electronic feedback," Journal of Micromechanics and Microengineering **25** (2015), 10.1088/0960-1317/25/4/045011.
[33]J. N. Reddy, *CRC Press .New York* (2003).
[34]F. Alijani and M. Amabili, "Theory and experiments for nonlinear vibrations of imperfect rectangular plates with free edges," Journal of Sound and Vibration **332**, 3564–3588 (2013).
[35]F. Alijani and M. Amabili, "Nonlinear vibrations of laminated and sandwich rectangular plates with free edges. Part 1: Theory and numerical simulations," Composite Structures **105**, 422–436 (2013).
[36]B. Baharlou and A. W. Leissa, "Vibration and buckling of generally laminated composite plates with arbitrary edge conditions," International Journal of Mechanical Sciences **29**, 545–555 (1987).
[37]C. W. BERT, "Unusual Poisson's ratios of pyrolytic graphite." AIAA Journal **7**, 1814–1815 (2008).
[38]A. Karvatskii, S. Leleka, T. Lazarev, and A. Pedchenko, "Investigation of the current state of isostatic graphite production technology," Technology audit and production reserves **2**, 16–21 (2017).
[39]H. Y. Erbil, "Evaporation of pure liquid sessile and spherical suspended drops: A review," (2012).
[40]M. A. Lombardi, *The Mechatronics Handbook: Chapter 17-Fundamentals of Time and Frequency* (2001) pp. 17.1–17.18.

Chapter 5

Conclusion

During the course of project, multiple findings and challenges were tackled. Firstly, the dynamical modelling of the flexural vibrations of a levitated plate was completed. It was found that the pyrolytic graphite plate exhibits a negative Poisson's ratio in-plane. The negative Poisson ratio in-plane of pyrolytic graphite is theorized to be due to wrinkling in the deposited layers of the pyrolytic carbon as similarly seen in graphene membranes. This finding was validated by extracting the material properties by minimizing the root mean square error between the modelled and experimentally obtained resonance frequencies. The negative Poisson ratio also explains the mode switching behaviour in comparison with the flexural modes of a levitating isostatic graphite plate with positive Poisson's ratio. The mass sensitivity of the levitating resonator was obtained by analysing the evaporation rate of water droplets and measuring frequency shifts associated with glass beads.

A phase lock loop was developed to analyse the frequency stability of the oscillator . The presence of drift was observed in the Allan deviation measurement and the root cause of the drift currently has not been identified. The precision for a square levitating oscillator of side length 2 mm was obtained to be 14.2 pg at a gate time of 0.1 s.

A patent for a diamagnetically levitated resonant mass sensor has been filed.
Patent Application Number: 2023462.
Filing Date : 09.09.2019.

5-1 Current Standing

The currently existing resonators for micro and nano particle measurement and their experimental and thermal noise based stability limits are presented by Sansa et al.[54]. The diamagnetically levitated oscillator developed in this work has been added for the purpose of giving an insight into its current standing based on the frequency stability of varying resonators in Figure 5-1.

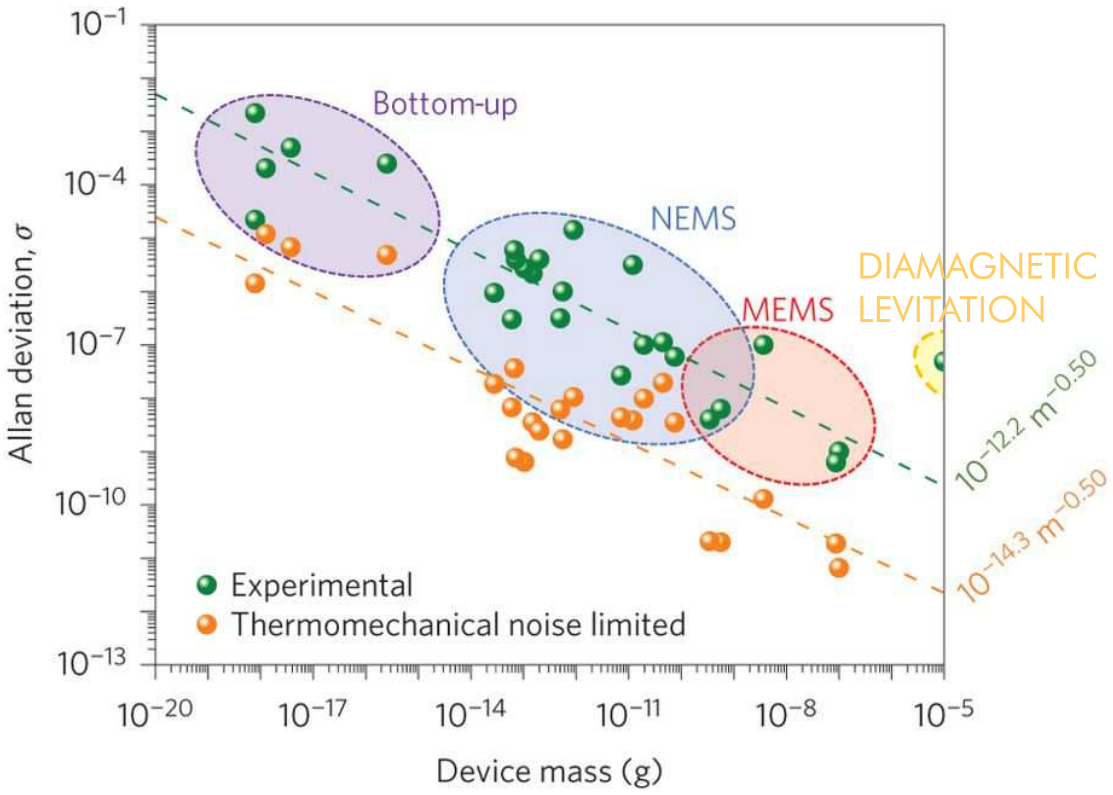

Figure 5-1: The comparison of different resonators in literature presented by Sansa et al.[54] with the addition of the diamagnetically levitated resonator developed in this work.

The diamagnetically levitated oscillator provides a low cost, disposable, robust and easy to use mass sensor in comparison with the MEMS and nanotube and nanowire based resonators. These resonators require expensive infrastructure, extreme working conditions (vacuum and low temperatures) and sophisticated setups for high mass sensitivity which makes it difficult to use. The diamagnetically levitated resonator on the other hand does not require sophisticated equipment, heavy infrastructure and is completely passive. The ease of assembly and its low cost based setup makes it a suitable technology with future potential as a point of care sensor for bio-medical research.

Chapter 6

Recommendations

Based on the learning throughout the course of the project, the recommendation for the future of the technology are presented below.

6-1 Point of Care Sensor

The diamagnetically levitated oscillator has the future potential to be developed as a low cost disposable point of care sensor for future bio-medical research. The first step for moving towards a better sensitivity is to understand and decrease the source of frequency noise in the system. A different readout mechanism such as a capacitive readout or an interferometric readout can lead to better frequency stability of the oscillator. The dynamical model of the phase lock loop should be developed for a better understanding of the different sources of noise and their effect on the system.

The effect of magnetic configurations on the stability of the device need to be studied and optimized for desired performance. The oscillator can be utilized to measure the stiffness and position of the added mass. The dimensions of the levitating oscillator can be reduced for better mass sensitivity.

Multiple levitating oscillators in combination with adaptive and swarm control can be developed as a one stop solution for the analysis of biological particles and dispersion of suitable medicines. It can be developed as a laboratory for artificial intelligence to conduct experiments without human interference as a long term goal[55].

The sensitivity of the levitating resonator needs to be computed in high temperature environments. The levitating plate can be put inside a heated chamber with the electronics and the magnets outside the chamber to prevent damage to the electronics. The levitated oscillator can also be developed as a mass sensor in liquids.

Chapter 7

Reflection

In this chapter, the reflection over the thesis procedure is elaborated along with the future outlook about the developed technology. The process overview elucidates the personal learning from the whole process along with the proposed and the followed timeline.

7-1 Project Formulation

This thesis project is a continuation in the field of research started by Ata Keşkekler in his master's thesis on rigid body dynamics of diamagnetically levitated objects. After the rigid body modelling, the proposal of working on analysing the flexural dynamics was put forth by Peter Steeneken and Farbod Alijani. The idea of developing a mass sensor utilizing the flexural dynamics was first investigated by a bachelor graduation project. Being a relatively new concept, the investigation of the flexural dynamics of diamagnetically levitated plates posed an interesting concept with wide ranging applications. This project thereby first focused on developing a mass sensor using a diamagnetically levitated resonator, being one of the major applications of MEMS resonators.

7-2 Learnings and Difficulties

The project was kicked off with direct experimentation since the beginning. It was crucial to get a basic understanding of the concept of diamagnetic levitation before proceeding with choosing the research question. Such a start was important to develop an intuition about the topic and get a good grasp of the basics.

The literature review helped in giving a sense of achievement and completion, also making the writing of the thesis at the end much easier. Presentation of the literature review along with the future plan in front of the group helped in receiving important feedback for the whole project.

It is quite easy to get distracted by multiple interesting phenomenon, so it is important to keep an end goal in mind while working. It is beneficial to make a task list intended to be completed at the beginning of the week with prioritization. Such planning helps in keeping the project structure intact.

Apart from these learnings, there were many different challenges that occurred during the course of the project. These challenges were not only limited to technical challenges, but were also sometimes more mental challenges. It is important to never hesitate in asking for advice and keeping an open mind for continuous learning and improvement. It is also important to not lose hope when stuck in a problem, but to take a break and look at it from a fresh perspective.

Apart from the technical challenges, I had to battle adverse health conditions to keep focused. And the support of my friends and family was of utmost importance to overcome these difficulties.

7-3 Work Timeline

The timeline of the project can be seen below in Figure 7-1.

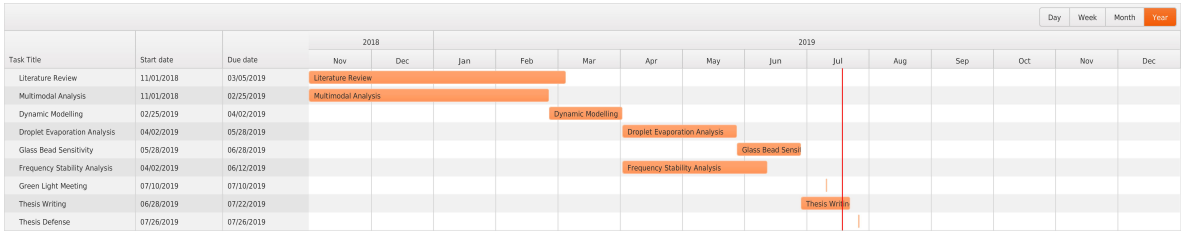

Figure 7-1: The timeline followed for the completion of the project

7-4 Future Outlook

The diamagnetically levitated resonator can have wide ranging applications as mass, position and stiffness sensor. The two major challenges for the further progress required to be solved is the manufacturing of smaller levitating plates and the reduction of noise of the resonator. The levitating resonator proves to be a very simple solution for mass sensing applications compared to other MEMS technologies.

Appendix A

Material Fabrication and Handling

This appendix explains in detail the different steps required for pyrolytic graphite (PG) sample preparation and handling while taking measurements; along with discussing the different techniques that were tried out during the course of the project for sample preparation.

A-1 Sample Preparation

The sample is first cleaved in thin slices with a scalpel for reducing the wastage of material due to polishing process. The second step to reduce the thickness of the sample is to sand the sample using fine grit size sandpaper obtained from the technicians at the PME lab. The next step requires the polishing of the graphite sample using the polishing machine available at the material science laboratory. After achieving a smooth surface polish, Optec laser cutter at the PME tower lab is used to cut the sample in required sizes.

WARNING:

- It is important to first fine tune the settings of the Optec laser cutter on a broken sample and ten proceed with the laser cutting of the main sample.
- It is also important to keep an eye on the laser cutting processes to check if the process finishes early, keeping in mind the parameters may vary with the dimensions of your required cut.
- A porous plate has been used for the laser cutting of the pyrolytic graphite sample to avoid layers of graphene getting removed every time the tape is removed.

The settings employed for the laser cutting of the pyrolytic graphite sample is stated in the table below.

Parameter	*Value*
Diode Current (A)	6
Drill Number	4
Drilling Step (mm)	0.01
No. of levels	25
Z Start (mm)	0
Z Step (mm)	-0.025
Speed	200
Jump Speed	200
Laser Firing Rate	35
Laser Power	100
Burst time	1000
Repetitions	700
Laser on delay	0
Laser off delay	0

Table A-1: Laser Cutter Settings for pyrolytic graphite plate of dimensions 4mmx4mmx0.1mm

A-2 Sample Handling

A gel box is utilized to keep the samples in good shape and order. The pick and place of the sample to the levitation stage and back; can be conducted with various techniques:

- Tweezers: Using tweezers to hold the sample pertain the risk of accidentally damaging the sample on application of too much force.
- Thin film (Paper/Polyimide): Based on the levitation height of the sample, a thin film is best suited for the picking and placing of the PG sample. The PG sample was placed on top of the polyimide film which was gently taken above the magnets, and slowly lowered causing the PG sample to levitation and the film was slowly removed from underneath. The picking up of the PG sample is done in a similar manner.
- Vacuum pen was utilized as well for picking up bigger samples, however due to nozzle size being bigger than the smaller samples, it was not used further.

A-2-1 Glass Beads: Pick and place

The glass beads are picked and placed on the PG sample using water beads. Water bead is obtained by filling a syringe with 30GA needle with water and gently pushing the handle to create a small water bead stuck to the needle. This water bead is then used to make contact with the glass bead in the petri dish and deposited on the PG sample. The PG sample is held down by applying pressure with a tweezer to overcome the capillary forces of the water bead.

A-3 Material Fabrication Trials

Different techniques were employed to obtain thinner and smaller samples out of which, sanding and laser cutting was finally utilized. The other approaches that were used were:

- Developing a composite filled with the carbon black obtained from sanding the pyrolytic graphite. The carbon black power was mixed with Clarocit powder and Clarocit liquid in 2:2:1 ratio to develop a composite material filled with carbon powder. This sample was unable to levitate over the varying magnetic configurations.
- Electrolytic etching utilizing LectroPol5 Tech of the pyrolytic graphite sample using KOH as the electrolyte was not successful.
- Isostatic graphite obtained from tokai carbon with a Poisson ratio of 0.23 and thickness of 0.5mm was obtained. It is possible to levitate this sample and its dynamic analysis proved that the negative poisson's ratio in fact causes mode switching.

Appendix B

Static Modelling

Diamagnetism is an inherent property of matter present in all materials. Diamagnetic materials develop an induced magnetic moment in the opposite direction of the applied magnetic field. Hence, they have negative magnetic susceptibilities. The force equilibrium in the z direction of a diamagnetically levitating object can be found by taking the gradient of the magnetic potential energy with gravity acting in the opposite direction[22].

$$\frac{1}{2\mu_0}\iiint_V \frac{\partial(\chi_x {B_x}^2 + \chi_y {B_y}^2 + \chi_z {B_z}^2)}{\partial z} dV = mg \tag{B-1}$$

where $\boldsymbol{\chi}$ is the diagonal magnetic susceptibility tensor, m is the mass of the object and $\vec{B}$ is the magnetic flux density.

The magnetic susceptibility of the pyrolytic graphite sheet is measured using a SQUID Magnetometer to measure the in plane and out of plane susceptibilities, the obtained susceptibilities are obtained by measuring the magnetization of the sample with varying magnetic flux density as shown in Figure B-1a. The obtained in plane magnetic susceptibility ($\chi_x = \chi_y$) is -6.08×10^{-5} and the out of plane susceptibility is -21.36×10^{-5}.

The levitation height of the pyrolytic graphite sheets of different side lengths were measured using Keyence digital microscope and compared with the heights obtained from the Finite Element model as shown in Figure B-1b.

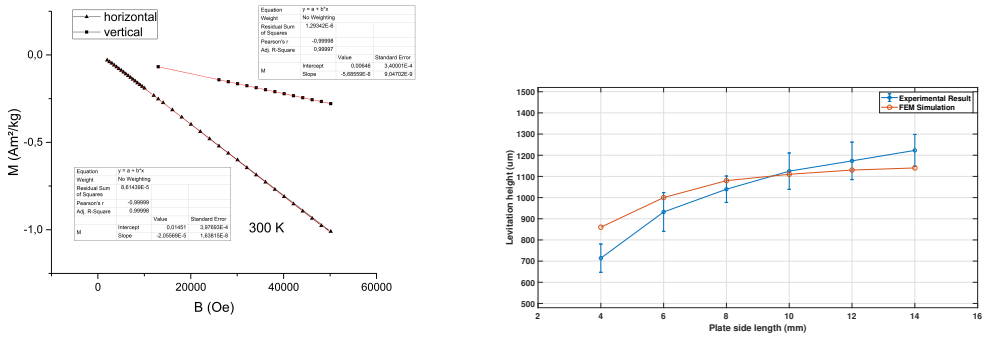

Figure B-1: a) The magnetic susceptibility measurement results obtained from the SQUID magnetometer. **b)** The levitation height of a pyrolytic graphite sheet levitating on top of a 2x2 diagonal levitation configuration in comparison with the obtained height from the finite element model.

The white light interferometer is utilized to measure the thickness of the pyrolytic graphite plates. The 3D contour and the surface profile the plates of side length 2 mm and 3 mm is shown in Figure B-2.

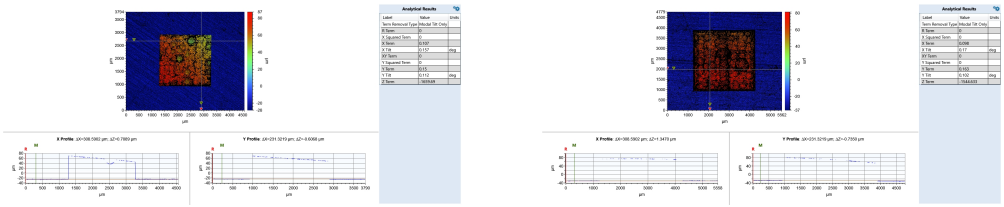

Figure B-2: The surface profile of pyrolytic graphite plates of side length 2mm and 3mm measured using white light interferometer.

Appendix C

Dynamics: Free Free Plate

This chapter provides the resonance frequencies obtained using the multi modal analysis conducted leveraging Polytech MSA 400 for the dynamical modelling of the free free plates to extract the material properties. Here, 4(1) is the plate used to compute the effective modal mass, droplet evaporation rate and Allan deviation; whereas 4(2) is the plate utilized for measuring the evaporation rate of low contact angle droplet by plasma cleaning.

Size (mm)	8	6	5	4(1)	4 (2)	2
Mode 1 (Hz)	5203	7529	10669	19710	20664	74200
Mode 2 (Hz)	7142	10026	14040	26359	27609	98593
Mode 3 (Hz)	7317	10681	14937	28164	29515	104656
Mode 4 (Hz)	12181	17443	24640	46828	48148	
Mode 5 (Hz)	12221	17809	25015		48595	
Mode 6 (Hz)		27091	38437			
Mode 7 (Hz)		28164	38773			
Mode 8 (Hz)	21476	31268	44210			
Mode 9 (Hz)		33713				
Mode 10 (Hz)		50393				
Mode 11 (Hz)		51709				

Appendix D

Sensitivity of levitated oscillator

Theta lite optical tensiometer was also used to measure the volume and contact angle evolution with time as shown in Figure D-1. The volume is seemed to be increasing with time. This error is attributed to the fact that the image processing software assumes substrate to be completely flat as the baseline, but the levitating plate with the water droplet is titled causing the error in measurement. Hence, these measurements were not utilized for droplet evaporation rate measurement. It is recommended to take the measurement on a static pyrolytic graphite plate for better readings.

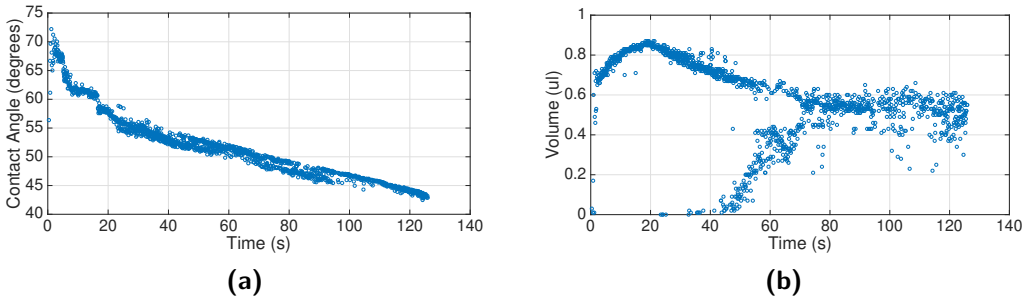

(a) **(b)**

Figure D-1: a) The contact angle versus time measurement for a droplet of initial volume 0.55ul measured using Theta lite optical tensiometer. **b)** The volume versus time measurement for a droplet of initial volume 0.55ul measured using Theta lite optical tensiometer.

The images of glass beads taken from the Polytech MSA 400 utilized for measuring the effective modal mass of the plates are shown in Figure D-2-D-4.

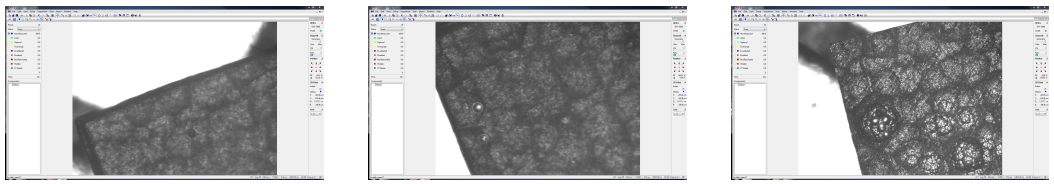

(a) (b) (c)

Figure D-2: The images of 1,2 and 4 beads respectively on a 2mm levitating plate utilized to obtain $M_{eff,exp}$

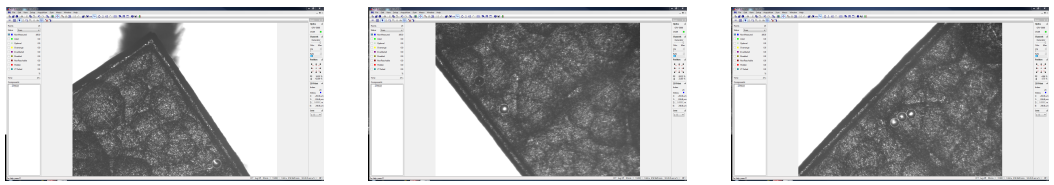

(a) (b) (c)

Figure D-3: The images of 1,2 and 3 beads respectively on a 3mm levitating plate utilized to obtain $M_{eff,exp}$

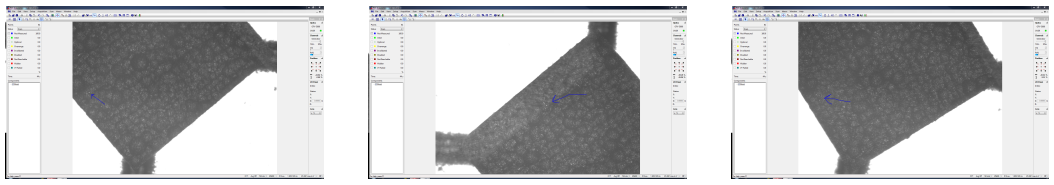

(a) (b) (c)

Figure D-4: The images of 1,2 and 3 beads respectively on a 4mm levitating plate utilized to obtain $M_{eff,exp}$

Bibliography

[1] E. H. Brandt, "Levitation in physics.," *Science (New York, N.Y.)*, vol. 243, pp. 349–55, jan 1989.

[2] H. Yaghoubi, "The most important maglev applications," mar 2013.

[3] H. W. Lee, K. C. Kim, and J. Lee, "Review of Maglev train technologies," jul 2006.

[4] B. V. Jayawant, "Review Lecture. Electromagnetic Suspension and Levitation Techniques," in *Proceedings of the Royal Society of London. Series A, Mathematical and Physical*, vol. 416, pp. 245–320, apr 1988.

[5] C. Pigot, H. Chetouani, G. Poulin, and G. Reyne, "Diamagnetic levitation of solids at microscale," in *IEEE Transactions on Magnetics*, vol. 44, pp. 4521–4524, nov 2008.

[6] D. E. G. Williams, "Magnetic Properties of Matter," *American Journal of Physics*, vol. 35, no. 9, p. 897, 1967.

[7] R. Feynman, R. Leighton, M. Sands, and S. Treiman, *The Feynman lectures on physics - Mainly Electromagnetism and Matter*. Addison-Wesley: Mass, 2010.

[8] R. Jackson, "John Tyndall and the Early History of Diamagnetism," oct 2015.

[9] S. L. O'Dell and R. K. P. Zia, "Classical and semiclassical diamagnetism: A critique of treatment in elementary texts," *American Journal of Physics*, vol. 54, pp. 32–35, jan 1986.

[10] S. Earnshaw, "On the nature of the molecular forces which regulate the constitution of the luminiferous ether," *Trans. Camb. Phil. Soc.*, vol. 7, no. Part I, pp. 97–112, 1842.

[11] M. D. Simon, L. O. Heflinger, and A. K. Geim, "Diamagnetically stabilized magnet levitation," *American Journal of Physics*, vol. 69, pp. 702–713, jun 2001.

[12] G. Kustler, "Diamagnetic levitation-Historical milestones," *REVUE ROUMAINE DES SCIENCES TECHNIQUES ...*, vol. 52, pp. 265–282, 2007.

[13] W. Braunbek, "Freischwebende Körper im elektrischen und magnetischen Feld," *Zeitschrift für Physik*, vol. 112, pp. 753–763, nov 1939.

[14] M. V. Berry and A. K. Geim, "Of flying frogs and levitrons," *European Journal of Physics*, vol. 18, pp. 307–313, jul 1997.

[15] M. D. Simon and A. K. Geim, "Diamagnetic levitation: Flying frogs and floating magnets (invited)," *Journal of Applied Physics*, vol. 87, pp. 6200–6204, apr 2000.

[16] A. Geim, "Everyone's magnetism," *Physics Today*, vol. 51, pp. 36–39, sep 1998.

[17] O. Cugat, J. Delamare, and G. Reyne, "Magnetic Micro-Actuators and Systems (MAGMAS)," *IEEE Transactions on Magnetics*, vol. 39, pp. 3607–3612, nov 2003.

[18] R. D. Waldron, "Diamagnetic levitation using pyrolytic graphite," *Review of Scientific Instruments*, vol. 37, pp. 29–35, jan 1966.

[19] I. Simon, A. G. Emslie, P. F. Strong, and R. K. McConnell, "Sensitive tiltmeter utilizing a diamagnetic suspension," *Review of Scientific Instruments*, vol. 39, pp. 1666–1671, nov 1968.

[20] E. Beaugnon and R. Tournier, "Levitation of water and organic substances in high static magnetic fields," *Journal de Physique III*, vol. 1, no. 8, pp. 1423–1428, 1991.

[21] E. Beaugnon, D. Fabregue, D. Billy, J. Nappa, and R. Tournier, "Dynamics of magnetically levitated droplets," *Physica B: Condensed Matter*, vol. 294-295, pp. 715–720, jan 2001.

[22] A. K. Geim and H. A. Ter Tisha, "Detection of earth rotation with a diamagnetically levitating gyroscope," *Physica B: Condensed Matter*, vol. 294-295, pp. 736–739, jan 2001.

[23] J. S. Brooks and J. A. Cothern, "Diamagnetism and magnetic force: A new laboratory for granular materials and chaotic/deterministic dynamics," *Physica B: Condensed Matter*, vol. 294, pp. 721–728, jan 2001.

[24] S. Verma, W. jong Kim, and J. Gu, "Six-axis nanopositioning device with precision magnetic levitation technoloy," *IEEE/ASME Transactions on Mechatronics*, vol. 9, pp. 384–391, jun 2004.

[25] R. E. Pelrine, "Room temperature, open-loop levitation of microdevices using diamagnetic materials," in *Micromechanics and MEMS: Classic and Seminal Papers to 1990*, pp. 320–323, IEEE, 1997.

[26] R. Pelrine, A. Wong-Foy, B. McCoy, D. Holeman, R. Mahoney, G. Myers, J. Herson, and T. Low, "Diamagnetically levitated robots: An approach to massively parallel robotic systems with unusual motion properties," in *Proceedings - IEEE International Conference on Robotics and Automation*, pp. 739–744, IEEE, may 2012.

[27] M. Kobayashi and J. Abe, "Optical motion control of maglev graphite," *Journal of the American Chemical Society*, 2012.

[28] S. Kang, J. Kim, J.-B. Pyo, J. H. Cho, and T.-S. Kim, "Design of Magnetic Force Field for Trajectory Control of Levitated Diamagnetic Graphite," *INTERNATIONAL JOURNAL OF PRECISION ENGINEERING AND MANUFACTURING-GREEN TECHNOLOGY*, vol. 5, no. 2, p. 341, 2018.

[29] I. F. Lyuksyutov, D. G. Naugle, and K. D. Rathnayaka, "On-chip manipulation of levitated femtodroplets," *Applied Physics Letters*, vol. 85, pp. 1817–1819, sep 2004.

[30] H. Chetouani, H. Rostaing, G. Reyne, C. Jeandey, V. Haguet, and C. Dieppedale, "Diamagnetic Levitation With Permanent Magnets for Contactless Guiding and Trapping of Microdroplets and Particles in Air and Liquids," *IEEE Transactions on Magnetics*, vol. 42, pp. 3557–3559, oct 2006.

[31] A. Cansiz and J. R. Hull, "Stable load-carrying and rotational loss characteristics of diamagnetic bearings," *IEEE Transactions on Magnetics*, vol. 40, pp. 1636–1641, may 2004.

[32] A. Cansiz, "Static and dynamic analysis of a diamagnetic bearing system," *Journal of Applied Physics*, vol. 103, p. 034510, feb 2008.

[33] W. Liu, W.-Y. Chen, W.-P. Zhang, X.-G. Huang, and Z.-R. Zhang, "Variable-capacitance micromotor with levitated diamagnetic rotor," *Electronics Letters*, vol. 44, no. 11, p. 681, 2008.

[34] Y. Su, Z. Xiao, Z. Ye, and K. Takahata, "Micromachined Graphite Rotor Based on Diamagnetic Levitation," *IEEE Electron Device Letters*, vol. 36, pp. 393–395, apr 2015.

[35] Y. Xu, Q. Cui, R. Kan, H. Bleuler, and J. Zhou, "Realization of a Diamagnetically Levitating Rotor Driven by Electrostatic Field," *IEEE/ASME Transactions on Mechatronics*, vol. 22, pp. 2387–2391, oct 2017.

[36] F. Barrot, J. Sandtner, and H. Bleuler, "Acceleration Sensor Based on Diamagnetic Levitation," *IUTAM Symposium on Vibration Control of Nonlinear Mechanisms and Structures*, pp. 81–90, 2005.

[37] D. Garmire, H. Choo, R. Kant, S. Govindjee, C. H. Séquin, R. S. Muller, and J. Demmel, "Diamagnetically levitated MEMS accelerometers," in *TRANSDUCERS and EUROSENSORS '07 - 4th International Conference on Solid-State Sensors, Actuators and Microsystems*, pp. 1203–1206, IEEE, 2007.

[38] G. De Pasquale, C. Siyambalapitiya, A. Somà, and J. Wang, "Performances improvement of MEMS sensors and energy scavengers by diamagnetic levitation," in *Proceedings of the 2009 International Conference on Electromagnetics in Advanced Applications, ICEAA '09*, pp. 465–468, IEEE, sep 2009.

[39] L. Liu and F. G. Yuan, "Nonlinear vibration energy harvester using diamagnetic levitation," *Applied Physics Letters*, vol. 98, p. 203507, may 2011.

[40] S. Palagummi and F. G. Yuan, "An optimal design of a mono-stable vertical diamagnetic levitation based electromagnetic vibration energy harvester," *Journal of Sound and Vibration*, vol. 342, pp. 330–345, apr 2015.

[41] S. Clara, H. Antlinger, A. Abdallah, E. Reichel, W. Hilber, and B. Jakoby, "An advanced viscosity and density sensor based on diamagnetically stabilized levitation," *Sensors and Actuators, A: Physical*, vol. 248, pp. 46–53, sep 2016.

[42] M. Boukallel, J. Abadie, E. Piat, and A. Savary, "Levitated micro-nano force sensor using diamagnetic materials magnetic materials," *Proceedings of the IEEE International Conference on Robotics and Automation*, vol. 3, pp. 3219–3224, 2003.

[43] Q. Li, K.-S. S. Kim, and A. Rydberg, "Lateral force calibration of an atomic force microscope with a diamagnetic levitation spring system," *Review of Scientific Instruments*, vol. 77, p. 065105, jun 2006.

[44] A. Keşkekler, *Characterization and Dynamics of Diamagnetically Levitated Objects*. PhD thesis, 2018.

[45] L. M. Hauzer, "Mass and stiffness measurement using a multi-modal analysis," 2017.

[46] M. S. Hanay, S. I. Kelber, C. D. O'Connell, P. Mulvaney, J. E. Sader, and M. L. Roukes, "Inertial imaging with nanomechanical systems," *Nature Nanotechnology*, vol. 10, no. 4, pp. 339–344, 2015.

[47] D. Ramos, J. Tamayo, J. Mertens, M. Calleja, L. G. Villanueva, and A. Zaballos, "Detection of bacteria based on the thermomechanical noise of a nanomechanical resonator: Origin of the response and detection limits," *Nanotechnology*, vol. 19, no. 3, pp. 35503–35512, 2008.

[48] H. Zhang and E. S. Kim, "Micromachined acoustic resonant mass sensor," *Journal of Microelectromechanical Systems*, vol. 14, pp. 699–706, aug 2005.

[49] R. Ruby, P. Bradley, Y. Oshmyansky, A. Chien, and J. Larson, "Thin film bulk wave acoustic resonators (FBAR) for wireless applications," in *2001 IEEE Ultrasonics Symposium. Proceedings. An International Symposium (Cat. No.01CH37263)*, vol. 1, pp. 813–821, IEEE, 2002.

[50] S. A. Zhgoon, A. S. Shvetsov, S. A. Sakharov, and O. Elmazria, "High-Temperature SAW Resonator Sensors: Electrode Design Specifics," *IEEE Transactions on Ultrasonics, Ferroelectrics, and Frequency Control*, vol. 65, pp. 657–664, apr 2018.

[51] J. Chaste, A. Eichler, J. Moser, G. Ceballos, R. Rurali, and A. Bachtold, "A nanomechanical mass sensor with yoctogram resolution," *Nature Nanotechnology*, vol. 7, pp. 301–304, may 2012.

[52] S. Kumar, "Fundamental Limits to Moore's Law," nov 2015.

[53] R. Fogel and J. Limson, "Developing biosensors in developing countries: South Africa as a case study," feb 2016.

[54] M. Sansa, E. Sage, E. C. Bullard, M. Gély, T. Alava, E. Colinet, A. K. Naik, L. G. Villanueva, L. Duraffourg, M. L. Roukes, G. Jourdan, and S. Hentz, "Frequency fluctuations in silicon nanoresonators," *Nature Nanotechnology*, vol. 11, pp. 552–558, jun 2016.

[55] V. Tshitoyan, J. Dagdelen, L. Weston, A. Dunn, Z. Rong, O. Kononova, K. A. Persson, G. Ceder, and A. Jain, "Unsupervised word embeddings capture latent knowledge from materials science literature," *Nature*, vol. 571, pp. 95–98, jul 2019.